Journal of Elasticity **65:** 87–129, 2001.

A Method Based on the Radon Transform for Three-Dimensional Elastodynamic Problems of Moving Loads

H.G. GEORGIADIS* and G. LYKOTRAFITIS
Mechanics Division, National Technical University of Athens, 1 Konitsis Street, Zographou GR-15773, Greece. E-mail: georgiad@central.ntua.gr

Received 14 June 2001; in revised form 6 December 2001

Abstract. An integral transform procedure is developed to obtain fundamental elastodynamic three-dimensional (3D) solutions for loads moving steadily over the surface of a half-space. These solutions are exact, and results are presented over the entire speed range (i.e., for subsonic, transonic and supersonic source speeds). Especially, the results obtained here for the tangential loads (one of these loads is along the direction of motion and the other is orthogonal to the direction of motion) are quite new in the literature. The solution technique is based on the use of the Radon transform and elements of distribution theory. It also fully exploits as auxiliary solutions the ones for the corresponding plane-strain and anti-plane shear problems (the latter problems are 2D and uncoupled from each other). In particular, it should be noticed that the plane-strain problem here is completely analogous to the original 3D problem, not only with respect to the field equations but also with respect to the boundary conditions. This makes the present technique more advantageous than other techniques, which require first the determination of a fictitious auxiliary plane-strain problem through the solution of an integral equation. Our approach becomes particularly simple when there is no angular dependence in the boundary conditions (i.e., when axially symmetric problems regarding their boundary conditions are considered). On the contrary, no such constraint needs to be fulfilled as regards the material response (and, therefore, the governing equations of the problem) and/or also possible loss of axisymmetry due to the generation of shock (Mach-type) waves in the medium. Therefore, the solution technique can easily deal with general 3D problems having a largely arbitrary radial dependence in the boundary conditions and involving: (i) material anisotropy in static and dynamic situations, and (ii) asymmetry caused by changes in the nature of governing PDEs due to the existence of different velocity regimes (super-Rayleigh, transonic, supersonic) in dynamic situations.

Key words: elastodynamics, moving loads, three-dimensional problems, Rayleigh waves, Radon transform, distributions.

1. Introduction

The *steady-state* elastodynamic problem of moving loads over the surface of a half-space has an interesting history over the last 50 years. It also enjoys important applications in the areas of Contact Mechanics and Wave Propagation (see, e.g., [1–7]). The simpler 2D problem was dealt with by Sneddon [8], Cole and

* Corresponding author.

Huth [9], and Georgiadis and Barber [10], among others, whereas the more difficult 3D problem by Eason [11], Lansing [6] and Barber [12]. In particular, the work in [10] corrects the Cole–Huth solution in the transonic range (the range where the velocity of the moving load is between the shear and longitudinal wave velocities), the work in [12] presents a superposition technique that reduces the original 3D problem to an auxiliary 2D problem, whereas the works in [6] and [11] employ double Fourier transforms. The latter two studies involve, however, a rather complicated analysis. Also, the study by Eason [11] considers both a normal load and a tangential load that has the direction of motion. However, this study is restricted to the sub-Rayleigh velocity range only. The studies by Lansing [6] and Barber [12] consider only normal concentrated loading but give results for the entire speed range. Finally, Brock and Rodgers [13] solved recently the more general *thermoelastic* 3D problem in the sub-Rayleigh range, via double two-sided Laplace transforms. Thus, it seems that there are no results available in the literature for the super-Rayleigh regime in the case of a tangential load having the direction of motion and for any velocity regime in the case of a tangential load that is orthogonal to the direction of motion.

The present study develops a method based on the Radon transform [14–16] and elements of distribution theory [17–19] to obtain a complete solution to the 3D steady-state problem of moving loads over the surface of an elastic half-space. The method fully exploits the solutions of corresponding 2D problems as auxiliary ones (these are two uncoupled problems, one plane-strain and one anti-plane shear). Indeed, after establishing the correspondence principle connecting the 3D problem with the two auxiliary problems, the solution to the original problem follows by performing first a coordinate transformation and then taking the inverse Radon transform of the known 2D solutions. Results are presented over the entire speed range (i.e., for sub-Rayleigh, super-Rayleigh/subsonic, transonic and supersonic speeds of the loads) and for both normal and tangential loading. The tangential loads are both in the direction of motion and orthogonal to that direction. In this way, not only a methodology is introduced here for attacking more general problems than the present 3D problem of *pure elastic* response of a half-space to moving surface loads (like, e.g., the corresponding coupled *thermoelastic* problem considered by the authors elsewhere [20] or problems involving moving indenters), but our results also fill a gap in the existing literature since we consider the cases of tangential loads and derive the expressions of tangential displacements in both cases of vertical and tangential loads.

It should be mentioned, of course, that another method which reduces 3D problems to 2D auxiliary ones, via superposition, was earlier introduced by Smirnov and Sobolev (see, e.g., [21, 22, 12]). This method, however, requires first the determination of a *fictitious* auxiliary plane-strain problem, which is obtainable only through the solution of an integral equation of the Abel type. Also, the solution to the aforementioned problem probably cannot be readily available in the literature since this auxiliary problem is somewhat artificial, as relative experience

indicates. On the contrary, it seems that the use of the Radon transform combined with a coordinate transformation *directly* leads to a reduction to a 2D situation that constitutes the analogue problem of the original 3D one. More specifically, it is shown that the corresponding plane-strain problem here is *completely* analogous to the original 3D problem, not only w.r.t. the field equations but also w.r.t. the boundary conditions. This makes the present technique (which is not based on explicit superposition-type arguments) more direct than the Smirnov–Sobolev technique.

Regarding the form of presentation of our results, we chose to give the results for the surface displacements in integral form, in most of the cases. Numerical evaluation of the integrals present no difficulty and it is performed by the numerical algorithms of MATHEMATICA™. Analytical considerations on these integrals (e.g., study of possible singularities of the integrands) are provided in the paper and show indeed that the integrals are amenable to a direct numerical treatment. Evaluating the integrals in closed analytical forms is possible only in the case of a normal displacement due to a normal force. This was done before by Barber [12] through some rather elaborate operations based on partial-fraction expansions and use of the Table of Gradshteyn and Ryzhik (see the Appendix of [12]). Our attempts to follow this procedure in the other cases treated here failed because the reduced integral forms are not available in the aforementioned Table nor they can be tackled *analytically* by MATHEMATICA™. However, nowadays, numerical treatment of integrals is routine and even if the present solution is utilized as a Green's function in a Boundary Integral Equation scheme such a treatment poses no difficulty in the code. Finally, we emphasize that both techniques, the one based on the Radon transform and the other based on superposition, provide the results in integral form; further treatment (either analytical or numerical) of the integrals has no relation with the techniques themselves.

Our approach becomes particularly simple when there is no angular dependence in the boundary conditions (i.e., when axially symmetric problems regarding their boundary conditions are considered). On the contrary, no such constraint needs to be fulfilled as regards the material response (and, therefore, the governing equations of the problem) and/or also possible loss of axisymmetry due to the generation of shock (Mach-type) waves in the medium. Therefore, the solution technique can easily deal with general 3D problems having a largely arbitrary radial dependence in the boundary conditions and involving: (i) material anisotropy in static and dynamic situations, and (ii) asymmetry caused by changes in the nature of governing PDEs due to the existence of different velocity regimes (super-Rayleigh, transonic, supersonic) in dynamic situations. The method still works in the case that the external loading is not axially symmetric but now the 2D auxiliary problems are not direct analogues of the original 3D problem.

In closing, we should also mention that interesting applications of the Radon transform in elasticity problems were presented before by Willis [23], Wang and Achenbach [24], and Shmegera [25], among others.

2. Problem Statement

Consider a linearly elastic isotropic body in the form of a 3D half-space $x_3 \geqslant 0$. This body is initially at rest but at time $t = 0$ a moving load starts to act upon it. The concentrated point load has components (S, T, P) along the axes (x_1, x_2, x_3), respectively, and moves under a constant velocity V over the surface $x_3 = 0$ and along the x_1-direction (see Figure 1). The equations of motion and the stress–strain relations with respect to a fixed Cartesian coordinate system $O'x_j$ $(j = 1, 2, 3)$ are written as

$$\mu\nabla^2\mathbf{u} + (\lambda + \mu)\nabla(\nabla \cdot \mathbf{u}) = \rho\frac{\partial^2\mathbf{u}}{\partial t^2}, \tag{1a}$$

$$\boldsymbol{\sigma} = \mu(\nabla\mathbf{u} + \mathbf{u}\nabla) + \lambda(\nabla \cdot \mathbf{u})\mathbf{1}, \tag{1b}$$

where $\mathbf{u}$ is the displacement vector with components u_j, $\boldsymbol{\sigma}$ is the stress tensor with components σ_{ij} $(i, j = 1, 2, 3)$, $\mathbf{1}$ is the identity tensor, ∇ is the gradient operator, $\nabla\cdot\mathbf{u}$ is the 3D dilatation, $\nabla^2 = (\partial^2/\partial x_1^2)+(\partial^2/\partial x_2^2)+(\partial^2/\partial x_3^2)$ is the 3D Laplacian operator, (λ, μ) are the Lamé constants, and ρ is the mass density.

We now introduce the standard *steady-state* assumption (see, e.g., [26, 27, 12, 13]) according to which a steady stress and displacement field is created in the medium w.r.t. an observer situated in a frame of reference attached to the moving load, if this source has been moving steadily for a sufficiently long time. In this way, any transients can reasonably be avoided (therefore gaining considerable

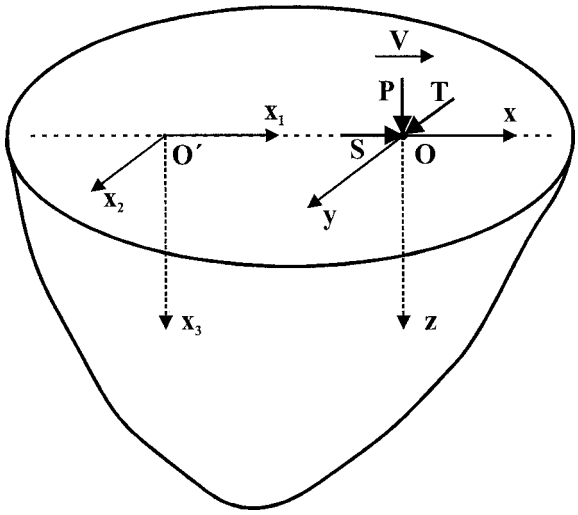

Figure 1. Point normal and tangential loads moving under constant velocity V over the surface of an elastic half-space. $O'x_1x_2x_3$ is a fixed Cartesian coordinate system and $Oxyz$ is a moving Cartesian coordinate system attached to the loads.

simplification in the analysis) and, moreover, upon introduction of the Galilean transformation

$$x = x_1 - Vt, \qquad y = x_2, \qquad z = x_3, \tag{2}$$

the boundary conditions become independent of t and the variables (x_1, t) enter the problem only in the combination $(x_1 - Vt)$. Furthermore, in the new moving Cartesian coordinate system $Oxyz$, partial derivatives w.r.t. t are neglected and (1a) can be written as

$$\nabla^2\mathbf{u} + (m^2 - 1)\nabla(\nabla \cdot \mathbf{u}) - m^2c^2\frac{\partial^2\mathbf{u}}{\partial x^2} = 0, \tag{3}$$

where $m = V_{\mathrm{L}}/V_{\mathrm{T}}$ with $V_{\mathrm{L}} = [(\lambda + 2\mu)/\rho]^{1/2}$ and $V_{\mathrm{T}} = (\mu/\rho)^{1/2}$ being, respectively, the longitudinal (L) and transverse (T) wave speeds, $c \equiv M_{\mathrm{L}} = V/V_{\mathrm{L}}$ and $mc \equiv M_{\mathrm{T}} = V/V_{\mathrm{T}}$ are the two *Mach* numbers, (u_x, u_y, u_z) are the components of the displacement vector, $\nabla \cdot \mathbf{u} = (\partial u_x/\partial x) + (\partial u_y/\partial y) + (\partial u_z/\partial z)$, and $\nabla^2 = (\partial^2/\partial x^2) + (\partial^2/\partial y^2) + (\partial^2/\partial z^2)$.

Finally, the boundary conditions of the problem take the form (see Figure 1)

$$\sigma_{zz}(x, y, z = 0) = -P\delta(x)\delta(y), \tag{4a}$$

$$\sigma_{zx}(x, y, z = 0) = -S\delta(x)\delta(y), \tag{4b}$$

$$\sigma_{zy}(x, y, z = 0) = -T\delta(x)\delta(y), \tag{4c}$$

which hold for $-\infty < x < +\infty$ and $-\infty < y < +\infty$. In the above equations, $(\sigma_{zx}, \sigma_{zy}, \sigma_{zz})$ are components of the stress tensor, and $\delta(\cdot)$ is the Dirac delta distribution. The objective of the ensuing analysis is to determine the displacement field for the problem described by equations (2)–(4).

3. Basic Radon-Transform Analysis

The solution of the previous problem will be obtained through a novel technique based on the Radon transform (see, e.g., [14–16]) and pertinent coordinate transformations. This general procedure reduces the original 3D problem to a pair of *auxiliary* problems, i.e., a corresponding 2D plane-strain problem and a 2D anti-plane shear problem. As will become apparent below, after establishing the *correspondence principle* between the 3D problem and the two auxiliary problems, the solution to the original problem follows simply by performing first a coordinate transformation and then taking the inverse Radon transform of the known plane-strain and anti-plane shear solutions. Since 2D problems are in general easier than their 3D counterparts, solutions to the auxiliary problems can be already available in many cases. Finally, the inversion operation relies upon results of distribution theory.

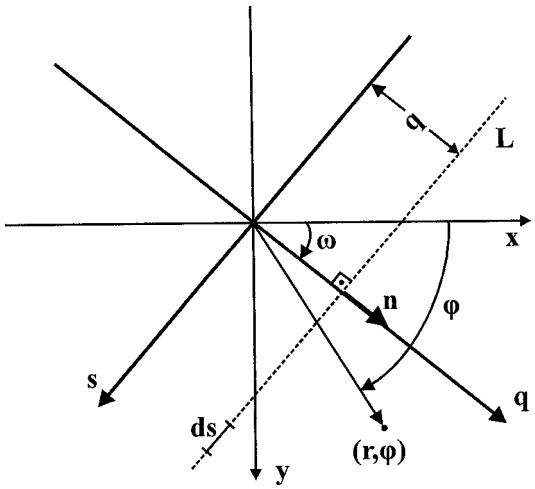

Figure 2. Geometry for the 2D Radon transform of functions in the xy-plane. The symbol L denotes all straight lines in the plane.

The 2D Radon transform of a function $f(\mathbf{r})$, with $|\mathbf{r}| = (x^2 + y^2)^{1/2}$, is defined as

$$\Re(f(\mathbf{r})) \equiv \tilde{f}(q,\omega) = \int\int f(\mathbf{r})\delta(q - \mathbf{n}\cdot\mathbf{r})\,\mathrm{d}\mathbf{r} = \int_L f(x,y)\,\mathrm{d}s$$
$$= \int_{-\infty}^{+\infty}\int_{-\infty}^{+\infty} f(x,y)\delta(q - x\cos\omega - y\sin\omega)\,\mathrm{d}x\,\mathrm{d}y, \tag{5}$$

where L denotes *all* straight lines in the plane Oxy (see Figure 2), and $\mathrm{d}s$ is the infinitesimal length along such a line. The lines L are defined by $\mathbf{n}\cdot\mathbf{r} = q$, with $\mathbf{n} \equiv (n_x, n_y) = (\cos\omega, \sin\omega)$, and the Radon transform is in fact the integral of $f(\mathbf{r})$ over all these straight lines in the plane.

The following three properties of the Radon transform are utilized in the present work:

(i) The *linearity* property is expressed as

$$\Re(C_1 f_1(\mathbf{r}) + C_2 f_2(\mathbf{r})) = C_1\tilde{f}_1(q,\omega) + C_2\tilde{f}_2(q,\omega), \tag{6}$$

where (C_1, C_2) are constants.

(ii) Rules for *derivative* transformations are written as

$$\Re\left(\frac{\partial f}{\partial x_j}\right) = n_j\frac{\partial\tilde{f}(q,\omega)}{\partial q}, \tag{7}$$

$$\Re\left(\frac{\partial^2 f}{\partial x_j\partial x_k}\right) = n_j n_k\frac{\partial^2\tilde{f}(q,\omega)}{\partial q^2}, \qquad \Re(\nabla^2 f) = \frac{\partial^2\tilde{f}(q,\omega)}{\partial q^2}, \tag{8a,b}$$

where the indices (j,k) take the values 1 and 2, $x_1 \equiv x$, $x_2 \equiv y$, and ∇^2 is now the 2D Laplace operator.

(iii) The transform of *multiplication* of Dirac delta distributions is

$$\Re\big(\delta(x)\cdot\delta(y)\big)=\delta(q). \tag{9}$$

Further, the inverse 2D Radon transform is given by

$$\begin{aligned} f(x,y) \;=\; f(r,\varphi) = -\frac{1}{4\pi^2}\int_0^{2\pi}\Bigg(\int_{-\infty}^{+\infty}\frac{\partial\tilde{f}(q,\omega)}{\partial q} \\ \times\,\mathbf{PF}\bigg(\frac{1}{q-r\cdot\cos(\omega-\varphi)}\bigg)\,\mathrm{d}q\Bigg)\,\mathrm{d}\omega, \end{aligned} \tag{10}$$

where the symbol **PF**() stands for the *principal-value* pseudo-function (or distribution) [17, 19] denoting that the inner integral is interpreted in the Cauchy principal-value sense [17, 28] due to a pole of the function inside the parenthesis. Equivalently, this distribution can be defined as

$$\big\langle\mathbf{PF}(1/x),\phi\big\rangle=\lim_{\varepsilon\to 0}\int_{|x|\geqslant\varepsilon}\frac{\phi(x)}{x}\,\mathrm{d}x,$$

where $\langle\cdot,\cdot\rangle$ denotes the inner product of distributions, ε is a positive real number and ϕ is a test function. In the analysis below, the case of more than one pole singularities in the same integrand (i.e., the case of a product of distributions) frequently appears and, therefore, the latter notation proves to be convenient.

Next, the two auxiliary problems will be obtained as transformed problems of the original problem. Operating with the Radon transform (5) to equations (3) and (4), and using the properties (6)–(9) gives

$$\frac{\partial^2\tilde{u}_x}{\partial q^2}+\frac{\partial^2\tilde{u}_x}{\partial z^2}+(m^2-1)n_x\frac{\partial}{\partial q}\bigg(n_x\frac{\partial\tilde{u}_x}{\partial q}+n_y\frac{\partial\tilde{u}_y}{\partial q}+\frac{\partial\tilde{u}_z}{\partial z}\bigg)-m^2c_x^2\frac{\partial^2\tilde{u}_x}{\partial q^2}=0, \tag{11a}$$

$$\frac{\partial^2\tilde{u}_y}{\partial q^2}+\frac{\partial^2\tilde{u}_y}{\partial z^2}+(m^2-1)n_y\frac{\partial}{\partial q}\bigg(n_x\frac{\partial\tilde{u}_x}{\partial q}+n_y\frac{\partial\tilde{u}_y}{\partial q}+\frac{\partial\tilde{u}_z}{\partial z}\bigg)-m^2c_x^2\frac{\partial^2\tilde{u}_x}{\partial q^2}=0, \tag{11b}$$

$$\frac{\partial^2\tilde{u}_z}{\partial q^2}+\frac{\partial^2\tilde{u}_z}{\partial z^2}+(m^2-1)\frac{\partial}{\partial z}\bigg(n_x\frac{\partial\tilde{u}_x}{\partial q}+n_y\frac{\partial\tilde{u}_y}{\partial q}+\frac{\partial\tilde{u}_z}{\partial z}\bigg)-m^2c_x^2\frac{\partial^2\tilde{u}_z}{\partial q^2}=0, \tag{11c}$$

$$\tilde{\sigma}_{zz}(q,\omega,z=0)=-P\cdot\delta(q), \tag{12a}$$

$$\tilde{\sigma}_{zx}(q,\omega,z=0)=-S\cdot\delta(q), \tag{12b}$$

$$\tilde{\sigma}_{zy}(q,\omega,z=0)=-T\cdot\delta(q), \tag{12c}$$

where $c_x=cn_x$. Now, as Figure 3 depicts, we perform a rotation of the original (x,y,z) coordinate system through an angle ω about the z-axis. In the new (q,s,z) coordinate system, equations (11)–(12) are expressed as

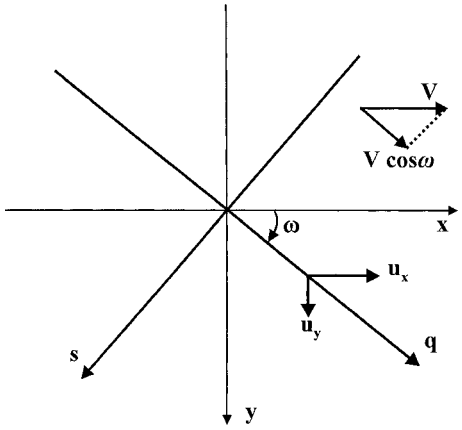

Figure 3. Initial xy-system and rotated qs-system.

$$\frac{\partial^2 \tilde{u}_q}{\partial q^2} + \frac{\partial^2 \tilde{u}_q}{\partial z^2} + (m^2 - 1)\frac{\partial}{\partial q}\left(\frac{\partial \tilde{u}_q}{\partial q} + \frac{\partial \tilde{u}_z}{\partial z}\right) - m^2 c_x^2 \frac{\partial^2 \tilde{u}_q}{\partial q^2} = 0, \tag{13a}$$

$$\frac{\partial^2 \tilde{u}_z}{\partial q^2} + \frac{\partial^2 \tilde{u}_z}{\partial z^2} + (m^2 - 1)\frac{\partial}{\partial z}\left(\frac{\partial \tilde{u}_q}{\partial q} + \frac{\partial \tilde{u}_z}{\partial z}\right) - m^2 c_x^2 \frac{\partial^2 \tilde{u}_z}{\partial q^2} = 0, \tag{13b}$$

$$(1 - m^2 c_x^2)\frac{\partial^2 \tilde{u}_s}{\partial q^2} + \frac{\partial^2 \tilde{u}_s}{\partial z^2} = 0, \tag{14}$$

$$\tilde{\sigma}_{zz}(q, \omega, z = 0) = -P \cdot \delta(q), \tag{15a}$$

$$\tilde{\sigma}_{zq}(q, \omega, z = 0) = -(S \cos\omega + T \sin\omega)\delta(q), \tag{15b}$$

$$\tilde{\sigma}_{zs}(q, \omega, z = 0) = (S \sin\omega - T \cos\omega)\delta(q), \tag{16}$$

where the following relations have been used

$$\begin{pmatrix} \tilde{u}_z \\ \tilde{u}_q \\ \tilde{u}_s \end{pmatrix} = \begin{pmatrix} 1 & 0 & 0 \\ 0 & \cos\omega & \sin\omega \\ 0 & -\sin\omega & \cos\omega \end{pmatrix} \begin{pmatrix} \tilde{u}_z \\ \tilde{u}_x \\ \tilde{u}_y \end{pmatrix}, \tag{17a}$$

$$\begin{pmatrix} \tilde{\sigma}_{zz} \\ \tilde{\sigma}_{zq} \\ \tilde{\sigma}_{zs} \end{pmatrix} = \begin{pmatrix} 1 & 0 & 0 \\ 0 & \cos\omega & \sin\omega \\ 0 & -\sin\omega & \cos\omega \end{pmatrix} \begin{pmatrix} \tilde{\sigma}_{zz} \\ \tilde{\sigma}_{zx} \\ \tilde{\sigma}_{zy} \end{pmatrix}. \tag{17b}$$

A crucial point of our analysis is the observation that the *rotated* Radon-transformed stresses and displacement gradients are related in exactly the same manner as in the physical (non-transformed) plane of the 2D plane-strain problem. Indeed, it can be proved, in view of (7) and (17), that the following relations hold

$$\tilde{\sigma}_{zz} = (\lambda + 2\mu)\frac{\partial \tilde{u}_z}{\partial z} + \lambda \frac{\partial \tilde{u}_q}{\partial q}, \tag{18a}$$

$$\tilde{\sigma}_{zq} = \mu\left(\frac{\partial \tilde{u}_z}{\partial q} + \frac{\partial \tilde{u}_q}{\partial z}\right), \tag{18b}$$

$$\tilde{\sigma}_{zs} = \mu \frac{\partial \tilde{u}_s}{\partial z}, \tag{19}$$

which obey the transformed Hooke's law $\tilde{\boldsymbol{\sigma}} = \mu(\nabla\tilde{\mathbf{u}} + \tilde{\mathbf{u}}\nabla) + \lambda(\nabla \cdot \tilde{\mathbf{u}})\mathbf{1}$, where $\tilde{\mathbf{u}}$ and $\tilde{\boldsymbol{\sigma}}$ have the components $(\tilde{u}_z, \tilde{u}_q, \tilde{u}_s)$ and $(\tilde{\sigma}_{zz}, \tilde{\sigma}_{zq}, \tilde{\sigma}_{zs}, \ldots)$, respectively.

Now, one may observe that equations (13), (15) and (18) form a 2D *plane-strain* problem in the (q, z) coordinate system. This problem (*first* auxiliary problem) involves a linearly elastic body in the form of the half-plane $z \geqslant 0$ that is disturbed by the steady-state motion of a concentrated plane line load. The load has components P and $(S\cos\omega + T\sin\omega)$ and is moving along the q-axis with velocity $V_q \equiv V\cos\omega$. On the other hand, equations (14), (16) and (19) form a 2D *anti-plane shear* problem in the (s, z) coordinate system. This problem (*second* auxiliary problem) involves a linearly elastic body in the form of the half-plane $z \geqslant 0$ that is disturbed by the steady-state motion of a concentrated anti-plane line load. In this case, the load $(S \cdot \sin\omega - T \cdot \cos\omega)$ is moving along the q-axis with velocity $V_q \equiv V\cos\omega$. Figure 4 depicts schematically the two auxiliary problems in the particular case of P and S loads.

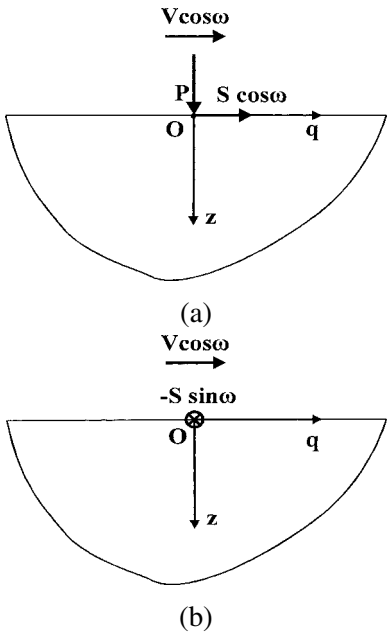

Figure 4. First (a) and second (b) auxiliary problems in the qz-plane. The case of (P, S) loading is considered.

4. Results for the First Auxiliary Problem

In this section, we record the solution of the first auxiliary problem (2D plane-strain problem) that was obtained before in the studies by Georgiadis and Barber [1, 10], and Brock and Georgiadis [29] (in the latter case as a limit of the more general coupled thermoelastic solution). Quantities in the physical plane in this auxiliary problem are, of course, *transformed* quantities in the Radon-transform plane of the original 3D problem. In using these results, care should be exercised in properly interpreting the 2D solution in the *rotated* coordinate system (i.e., in retaining the physics of the solution in the new system). More details on the latter issue are given in the end of the present section.

By superposition, the total *normal* displacement at the surface, in the entire speed range, is written as

$$\begin{aligned}\tilde{u}_z(q,\omega,z=0) \;=\; & \tilde{u}_z^{(P)}(q,\omega,z=0)+\tilde{u}_z^{(S)}(q,\omega,z=0)\\ & +\tilde{u}_z^{(T)}(q,\omega,z=0),\end{aligned} \tag{20}$$

where the normal surface displacement $\tilde{u}_z^{(P)}$ due to a normal load P is given by

$$\begin{aligned}\tilde{u}_z^{(P)}(q,\omega,z=0) \;=\; & \frac{P}{\mu}\Bigg[F_1^{(P)}(M_{\mathrm{T}}\cos\omega)\cdot\ln(|q|)\\ & -\frac{F_2^{(P)}(M_{\mathrm{T}}\cos\omega)}{2}\cdot\mathrm{sgn}\Big(\mathrm{sgn}(\cos\omega)\cdot q\Big)\Bigg],\end{aligned} \tag{21}$$

the normal displacement $\tilde{u}_z^{(S)}$ due to a tangential load $S\cos\omega$ by

$$\begin{aligned}\tilde{u}_z^{(S)}(q,\omega,z=0) \;=\; & \frac{S\cos\omega\cdot\mathrm{sgn}(\cos\omega)}{\mu}\Bigg[F_1^{(S)}(M_{\mathrm{T}}\cos\omega)\cdot\ln(|q|)\\ & -\frac{F_2^{(S)}(M_{\mathrm{T}}\cos\omega)}{2}\cdot\mathrm{sgn}(\mathrm{sgn}(\cos\omega)\cdot q)\Bigg],\end{aligned} \tag{22a}$$

and the normal displacement $\tilde{u}_z^{(T)}$ due to a tangential load $T\sin\omega$ by

$$\begin{aligned}\tilde{u}_z^{(T)}(q,\omega,z=0) \;=\; & \frac{T\sin\omega\cdot\mathrm{sgn}(\sin\omega)}{\mu}\Bigg[F_1^{(S)}(M_{\mathrm{T}}\cos\omega)\cdot\ln(|q|)\\ & -\frac{F_2^{(S)}(M_{\mathrm{T}}\cos\omega)}{2}\cdot\mathrm{sgn}(\mathrm{sgn}(\cos\omega)\cdot q)\Bigg],\end{aligned} \tag{22b}$$

where sgn( ) is the signum function, and

$$F_1^{(P)}(M_{\mathrm{T}})=\begin{cases}\dfrac{M_{\mathrm{T}}^2(1-M_{\mathrm{L}}^2)^{1/2}}{\pi R(M_{\mathrm{T}})}\equiv F_{11}^{(P)}(M_{\mathrm{T}}), & V<V_{\mathrm{T}},\\[2ex] \dfrac{M_{\mathrm{T}}^2(2-M_{\mathrm{T}}^2)^2(1-M_{\mathrm{L}}^2)^{1/2}}{\pi K(M_{\mathrm{T}})}\equiv F_{12}^{(P)}(M_{\mathrm{T}}), & V_{\mathrm{T}}<V<V_{\mathrm{L}},\\[2ex] 0\equiv F_{13}^{(P)}(M_{\mathrm{T}}), & V_{\mathrm{L}}<V,\end{cases} \tag{23}$$

$$F_2^{(P)}(M_{\mathrm{T}}) = \begin{cases} 0 \equiv F_{21}^{(P)}(M_{\mathrm{T}}), & V < V_{\mathrm{T}}, \\ \dfrac{4M_{\mathrm{T}}^2(1-M_{\mathrm{L}}^2)(M_{\mathrm{T}}^2-1)^{1/2}}{K(M_{\mathrm{T}})} \equiv F_{22}^{(P)}(M_{\mathrm{T}}), & V_{\mathrm{T}} < V < V_{\mathrm{L}}, \\ \dfrac{M_{\mathrm{T}}^2(M_{\mathrm{L}}^2-1)^{1/2}}{N(M_{\mathrm{T}})} \equiv F_{23}^{(P)}(M_{\mathrm{T}}), & V_{\mathrm{L}} < V, \end{cases} \tag{24}$$

$$F_1^{(S)}(M_{\mathrm{T}}) = \begin{cases} 0 \equiv F_{11}^{(S)}(M_{\mathrm{T}}), \quad V < V_{\mathrm{T}}, \\ -\dfrac{2M_{\mathrm{T}}^2(2-M_{\mathrm{T}}^2)(1-M_{\mathrm{L}}^2)^{1/2}(M_{\mathrm{T}}^2-1)^{1/2}}{\pi K(M_{\mathrm{T}})} \equiv F_{12}^{(S)}(M_{\mathrm{T}}), \\ \quad V_{\mathrm{T}} < V < V_{\mathrm{L}}, \\ 0 \equiv F_{13}^{(S)}(M_{\mathrm{T}}), \quad V_{\mathrm{L}} < V, \end{cases} \tag{25}$$

$$F_2^{(S)}(M_{\mathrm{T}}) = \begin{cases} \dfrac{(2-M_{\mathrm{T}}^2) - 2(1-M_{\mathrm{L}}^2)^{1/2}(1-M_{\mathrm{T}}^2)^{1/2}}{R(M_{\mathrm{T}})} \equiv F_{21}^{(S)}(M_{\mathrm{T}}), \\ \quad V < V_{\mathrm{T}}, \\ \dfrac{(2-M_{\mathrm{T}}^2)^3 + 8(1-M_{\mathrm{L}}^2)(M_{\mathrm{T}}^2-1)}{K(M_{\mathrm{T}})} \equiv F_{22}^{(S)}(M_{\mathrm{T}}), \\ \quad V_{\mathrm{T}} < V < V_{\mathrm{L}}, \\ \dfrac{(2-M_{\mathrm{T}}^2) + 2(M_{\mathrm{L}}^2-1)^{1/2}(M_{\mathrm{T}}^2-1)^{1/2}}{N(M_{\mathrm{T}})} \equiv F_{23}^{(S)}(M_{\mathrm{T}}), \\ \quad V_{\mathrm{L}} < V, \end{cases} \tag{26}$$

the latter four functions being defined as functions of the 'shear' (or 'transverse') Mach number M_{T}. Notice that M_{L} and M_{T} are related, by their definition, through the following equation

$$M_{\mathrm{L}} = \frac{1}{m} M_{\mathrm{T}}, \qquad m \equiv \frac{V_{\mathrm{L}}}{V_{\mathrm{T}}} = \left[\frac{2(1-\nu)}{1-2\nu}\right]^{1/2} > 1, \tag{27a,b}$$

where ν is the Poisson ratio of the material. Also, in the above equations

$$R(M_{\mathrm{T}}) = (2-M_{\mathrm{T}}^2)^2 - 4(1-M_{\mathrm{L}}^2)^{1/2}(1-M_{\mathrm{T}}^2)^{1/2}, \tag{28}$$

is the *steady-state* Rayleigh function (see, e.g., [9, 1, 30]) defining the Rayleigh-wave speed V_{R} by $R(V_{\mathrm{R}}/V_{\mathrm{T}}) = 0$, and

$$N(M_{\mathrm{T}}) = \left(2-M_{\mathrm{T}}^2\right)^2 + 4\left(M_{\mathrm{L}}^2-1\right)^{1/2}\left(M_{\mathrm{T}}^2-1\right)^{1/2}, \tag{29a}$$

$$K(M_{\mathrm{T}}) = \left(2-M_{\mathrm{T}}^2\right)^4 - 16\left(1-M_{\mathrm{L}}^2\right)\left(1-M_{\mathrm{T}}^2\right), \tag{29b}$$

where the latter function, in particular, results as a product by the multiplication of complex conjugates involving the Rayleigh function, at a certain step in the solution procedure. Appendix A of the present work provides a brief analysis concerning the zeroes of $K(M_{\mathrm{T}})$. These results were obtained in the spirit of the work of Rachman and Barber [30].

In the same fashion now, one can write by superposition the total *tangential* displacement at the surface. In this case, in order to avoid the presentation of complicated results we chose to deal only with the subsonic problem. Therefore, the results below for the 2D auxiliary problem are for the speed range $V < V_{\mathrm{T}}$. We also avoid the less practical case of the T load and consider only the loading (P, S). Indeed, it is difficult for one to apply and maintain a moving load having a direction that is orthogonal to the direction of motion. Accordingly, one may write

$$\tilde{u}_q(q, \omega, z = 0) = \tilde{u}_q^{(P)}(q, \omega, z = 0) + \tilde{u}_q^{(S)}(q, \omega, z = 0), \tag{30}$$

where the tangential surface displacement $\tilde{u}_q^{(P)}$ due to a normal load P is given by

$$\tilde{u}_q^{(P)}(q, \omega, z = 0) = -\frac{P \cdot \operatorname{sgn}(\cos\omega)}{2\mu} G^{(P)}(M_{\mathrm{T}} \cos\omega) \cdot \operatorname{sgn}(\operatorname{sgn}(\cos\omega) \cdot q), \tag{31}$$

and the tangential surface displacement $\tilde{u}_q^{(S)}$ due to a tangential load $S \cdot \cos\omega$ by

$$\tilde{u}_q^{(S)}(q, \omega, z = 0) = \frac{S \cos\omega}{\mu} G^{(S)}(M_{\mathrm{T}} \cos\omega) \cdot \ln(|q|). \tag{32}$$

Again, functions of M_{T} enter the solution. These are defined as follows

$$G^{(P)}(M_{\mathrm{T}}) = -\frac{(2 - M_{\mathrm{T}}^2) - 2(1 - M_{\mathrm{L}}^2)^{1/2}(1 - M_{\mathrm{T}}^2)^{1/2}}{R(M_{\mathrm{T}})}, \quad V < V_{\mathrm{T}}, \tag{33}$$

$$G^{(S)}(M_{\mathrm{T}}) = \frac{M_{\mathrm{T}}^2(1 - M_{\mathrm{T}}^2)^{1/2}}{\pi R(M_{\mathrm{T}})}, \qquad V < V_{\mathrm{T}}. \tag{34}$$

At this point, we should provide an explanation of the way that the results from the physical plane-strain problem [1, 10, 29] have been transferred to the first auxiliary problem. The solution to the physical problem contains the function $\operatorname{sgn}(x)$, and in order to preserve this behavior in the auxiliary problem we should have a Radon transformed solution containing the function $\operatorname{sgn}(q)$ when $\omega \in [0, \pi/2) \cup (3\pi/2, 2\pi]$(this is because the projection, $V_q = V \cdot \cos\omega$, of the velocity V on the q-axis has a positive direction) and the function $\operatorname{sgn}(-q)$ when $\omega \in (\pi/2, 3\pi/2)$ (because now the projection has a negative direction). In a compact form, the Radon transformed solution (i.e., the solution to the first auxiliary problem) that corresponds to the behavior $\operatorname{sgn}(x)$ of the physical plane-strain solution is written as $\operatorname{sgn}(\operatorname{sgn}(\cos\omega) \cdot q)$ (cf. Equations (21), (22) and (31)). In addition, Figures 5(a) and 5(b) depict the first auxiliary problem and the behavior

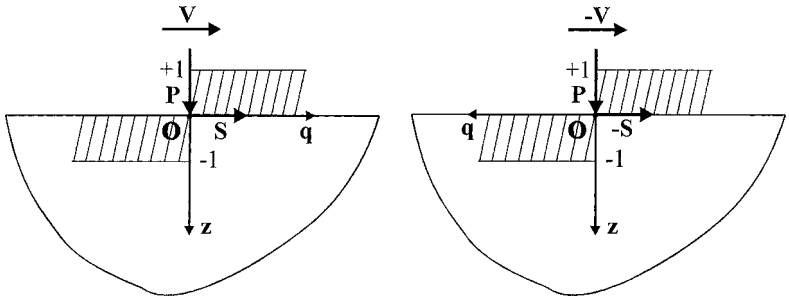

(a) (b)

Figure 5. Schematics for the first auxiliary problem and behavior of the function $\operatorname{sgn}(\operatorname{sgn}(\cos\omega)\cdot q)$ in the cases $\omega = 0$ (a) and $\omega = \pi$ (b).

of the function $\operatorname{sgn}(\operatorname{sgn}(\cos\omega)\cdot q)$ for the special cases $\omega = 0$ and $\omega = \pi$, respectively. On the contrary, no special care should be exercised about the 'transfer' of $\ln|q|$ since this is an even function. Finally, one should take into account the *possible* influence of the rotation of the coordinate system upon the direction of the displacements. For instance, the load S in the solution $u_z^{(S)}$ of the physical problem should be taken as $S\cos\omega\cdot\operatorname{sgn}(\cos\omega)$, instead of the projection $S_q \equiv S\cos\omega$, in the auxiliary problem.

5. Solution of the Second Auxiliary Problem

It seems that the solution to the second auxiliary problem, i.e., the surface displacement in the half-plane $z \geqslant 0$ due to a moving anti-plane shear load, does not exist in the literature. This solution was obtained in the course of the present investigation and is briefly presented in Appendix B. The integral-transform procedure of Brock and Georgiadis [29] was followed.

In the anti-plane shear case, only two speed ranges exist (i.e., the subsonic range $|V\cos\omega| < V_{\mathrm{T}}$ and the supersonic $|V\cos\omega| > V_{\mathrm{T}}$ range of the load motion w.r.t. the velocity V_{T}). In the entire regime, the solution is given in a compact form as

$$\tilde{u}_s^{(S)}(q,\omega,z=0) = \frac{S\cdot\sin\omega}{\mu}\big[Q_1\big(M_{\mathrm{T}}\cos\omega\big)\ln(|q|) + Q_2(M_{\mathrm{T}}\cos\omega)H(-\operatorname{sgn}(\cos\omega)\cdot q)\big], \tag{35}$$

where $H()$ is the Heaviside step function, and

$$Q_1(M_{\mathrm{T}}) = \begin{cases} \dfrac{1}{\pi(1-M_{\mathrm{T}}^2)^{1/2}} \equiv Q_{11}(M_{\mathrm{T}}), & V < V_{\mathrm{T}}, \\ 0 \equiv Q_{12}(M_{\mathrm{T}}), & V > V_{\mathrm{T}}, \end{cases} \tag{36}$$

$$Q_2(M_{\mathrm{T}}) = \begin{cases} 0 \equiv Q_{21}(M_{\mathrm{T}}), & V < V_{\mathrm{T}}, \\ -\dfrac{1}{(M_{\mathrm{T}}^2-1)^{1/2}} \equiv Q_{22}(M_{\mathrm{T}}), & V > V_{\mathrm{T}}, \end{cases} \tag{37}$$

Notice in (35) and for the supersonic case that the argument q of the step function is multiplied by $\mathrm{sgn}(\cos\omega)$ in order for the surface disturbances to be always *behind* the source and not ahead, as the velocity component V_q changes sign in the course of the Radon-transform inversion. Moreover, in utilizing the physical solution in the transformed plane, we take into account that the direction of the displacement $\tilde{u}_s$ does not depend upon the direction of the motion of the load but does depend upon the direction of the projection of the shear load $S_s \equiv -S \cdot \sin\omega$.

It is noticed finally that in the case of only a vertical load P acting upon the half-space surface (in the original 3D problem), the solution to the second auxiliary problem is $\tilde{u}_s(q, \omega, z = 0) \equiv 0$ since $\tilde{\sigma}_{zs}(q, \omega, z = 0) = 0$ is to be taken as a boundary condition.

6. Inversion Procedure and Results for the Actual Problem

The 3D solution follows from the transformed solution in two steps. First, the inversion of the coordinate transformation in (17) is performed providing the set $(\tilde{u}_z, \tilde{u}_x, \tilde{u}_y)$ in terms of the rotated Radon-transformed displacements $(\tilde{u}_z, \tilde{u}_q, \tilde{u}_s)$, i.e.,

$$\begin{pmatrix} \tilde{u}_z \\ \tilde{u}_x \\ \tilde{u}_y \end{pmatrix} = \begin{pmatrix} 1 & 0 & 0 \\ 0 & \cos\omega & -\sin\omega \\ 0 & \sin\omega & \cos\omega \end{pmatrix} \begin{pmatrix} \tilde{u}_z \\ \tilde{u}_q \\ \tilde{u}_s \end{pmatrix}. \tag{38}$$

Then, the Radon-transform inversion according to (10) gives the set (u_z, u_x, u_y) in the physical plane. Finally, from the latter solution, one can calculate the displacements in a system of cylindrical polar coordinates (r, φ, z) by using the coordinate transformation (see Figure 6)

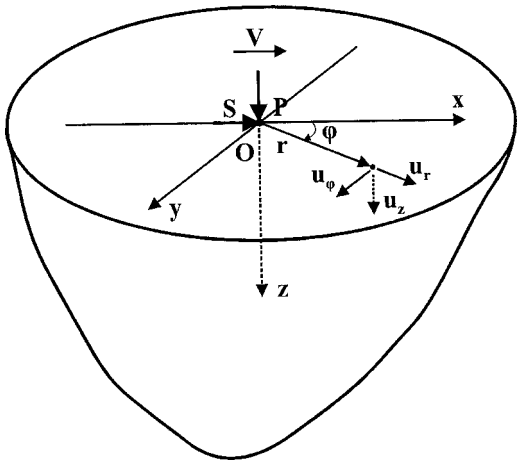

Figure 6. System of cylindrical polar coordinates (r, φ, z) and corresponding displacement components.

$$\begin{pmatrix} u_z \\ u_r \\ u_\varphi \end{pmatrix} = \begin{pmatrix} 1 & 0 & 0 \\ 0 & \cos\varphi & \sin\varphi \\ 0 & -\sin\varphi & \cos\varphi \end{pmatrix} \begin{pmatrix} u_z \\ u_x \\ u_y \end{pmatrix}, \tag{39}$$

and also evaluate the stresses through (1b).

By invoking superposition and in order to avoid presenting complicated results, we consider separately the displacements due to the vertical load P and the displacements due to the tangential load S.

6.1. VERTICAL DISPLACEMENT $u_z^{(P)}$ DUE TO THE VERTICAL LOAD P

The rotation of the original coordinate system (x, y, z) does not affect the transformed component $\tilde{u}_z$, as is obvious from (17a), and therefore the second auxiliary problem does not play a role here. Accordingly, operating with the inverse Radon transform (equation (10)) on (21) and using the following relations from the theory of generalized functions [17]

$$\frac{\partial \operatorname{sgn}(\operatorname{sgn}(\cos\omega)\cdot q)}{\partial q} = 2\operatorname{sgn}(\cos\omega)\cdot\delta(q), \tag{40}$$

$$\frac{\partial \ln(|q|)}{\partial q} = \mathbf{PF}\left(\frac{1}{q}\right), \tag{41}$$

we obtain

$$\begin{aligned} u_z^{(P)}(r,\varphi,z=0) \;=\; & -\frac{P}{4\pi^2\mu}\left\{ \int_0^{2\pi} \left[F_1^{(P)}(M_\mathrm{T}\cos\omega) \right.\right. \\ & \times\left(\int_{-\infty}^{+\infty} \mathbf{PF}\left(\frac{1}{q}\right)\cdot \mathbf{PF}\left(\frac{1}{q - r\cos(\omega-\varphi)}\right) \mathrm{d}q \right) \Big] \mathrm{d}\omega \\ & - \int_0^{2\pi} \left[\operatorname{sgn}(\cos\omega)\cdot F_2^{(P)}(M_\mathrm{T}\cos\omega) \right. \\ & \left.\left. \times\left(\int_{-\infty}^{+\infty} \mathbf{PF}\left(\frac{1}{q - r\cos(\omega-\varphi)}\right)\cdot\delta(q)\,\mathrm{d}q \right) \right] \mathrm{d}\omega \right\}. \end{aligned} \tag{42}$$

An important point to notice here is that any *rigid-body* displacement terms, which could be added in the RHS of (21), have been eliminated by differentiation in the process of the Radon-transform inversion. Further, the evaluation of the inner integrals is accomplished by utilizing results from Lauwerier [18], which concern the Hilbert transform of generalized functions, i.e.,

$$\int_{-\infty}^{+\infty} \mathbf{PF}\left(\frac{1}{q}\right)\cdot \mathbf{PF}\left(\frac{1}{q - r\cos(\omega-\varphi)}\right) \mathrm{d}q = \pi^2\delta\big(r\cos(\omega-\varphi)\big), \tag{43}$$

$$\int_{-\infty}^{+\infty} \mathbf{PF}\left(\frac{1}{q - r\cos(\omega-\varphi)}\right)\cdot\delta(q)\,\mathrm{d}q = -\mathbf{PF}\left(\frac{1}{r\cos(\omega-\varphi)}\right). \tag{44}$$

With the above results in hand, equation (42) becomes

$$u_z^{(P)}(r,\varphi,z=0) = -\frac{P}{4\mu}\left\{\int_0^{2\pi}\left[F_1^{(P)}(M_\mathrm{T}\cos\omega)\cdot\delta(r\cos(\omega-\varphi))\right]\mathrm{d}\omega + \int_0^{2\pi}\left[\mathrm{sgn}(\cos\omega)\cdot F_2^{(P)}(M_\mathrm{T}\cos\omega)\cdot\mathbf{PF}\left(\frac{1}{\pi^2 r\cos(\omega-\varphi)}\right)\right]\mathrm{d}\omega\right\}. \quad (45)$$

Now, two properties of the Dirac delta distribution will be employed, namely the sifting property and the property that

$$\delta[g(x)] = \sum_{j=1}^{N}\frac{\delta(x-a_j)}{|g'(a_j)|},$$

where $g(x)$ is a monotonic function of x which vanishes at the points $x = a_j$, with $(j = 1, 2, \ldots, N)$, and $g'(a_j)$ are the derivatives at the points $x = a_j$. These two properties lead to the value $(2/r)F_1^{(P)}(M_\mathrm{T}\sin\varphi)$ for the first integral in (45). Also, the second integral is transformed through the monotonic change of variable $\zeta = \sin\omega$. Equation (45) therefore becomes

$$u_z^{(P)}(r,\varphi,z=0) = -\frac{P}{\mu r}\left\{\frac{1}{2}F_1^{(P)}(M_\mathrm{T}\sin\varphi) + \frac{\cos\varphi}{\pi^2}\times\left[\int_0^1 F_2^{(P)}\big(M_\mathrm{T}(1-\zeta^2)^{1/2}\big)\mathbf{PF}\left(\frac{1}{\cos^2\varphi-\zeta^2}\right)\mathrm{d}\zeta\right]\right\}. \quad (46)$$

This is a key result of the present analysis. From this result, particular results will be obtained below for the entire speed range, i.e., for $0 < V < V_\mathrm{R}$, $V_\mathrm{R} < V < V_\mathrm{T}$, $V_\mathrm{T} < V < V_\mathrm{L}$ and $V_\mathrm{L} < V$. The particular results depend of course upon the forms of the functions $F_1^{(P)}()$ and $F_2^{(P)}()$ in each speed range. Finally, one may notice in (46) that the surface vertical displacement $u_z^{(P)}$ is indeed symmetric with respect to the x-axis.

6.1.1. *Sub-Rayleigh Range* $(0 < V < V_\mathrm{R})$

Here, only the first term in the RHS of (46) contributes, since $F_2^{(P)}(M_\mathrm{T}(1-\zeta^2)^{1/2}) = 0$ for all $\zeta \in [0, 1]$. Thus, the final result is

$$u_z^{(P)}(r,\varphi,z=0) = -\frac{P}{2\mu r}F_{11}^{(P)}(M_\mathrm{T}\sin\varphi), \quad (47)$$

where the function $F_{11}^{(P)}()$ was defined in (23). One may observe from (47) that $u_z^{(P)}$ exhibits symmetry w.r.t. both axes x and y.

6.1.2. *Super-Rayleigh Subsonic Range* $(V_\mathrm{R} < V < V_\mathrm{T})$

The solution is still given by the first term in the RHS of (46). However, as the analysis in Appendix A indicates, along the lines $\varphi = \pm\varphi_\mathrm{R}$ and $\varphi = \pi \pm \varphi_\mathrm{R}$ on the half-space surface (with $\varphi_\mathrm{R} = \sin^{-1}(m_1^{1/2}/M_\mathrm{T})$ and $0 < \varphi_\mathrm{R} < \pi/2$), the Rayleigh

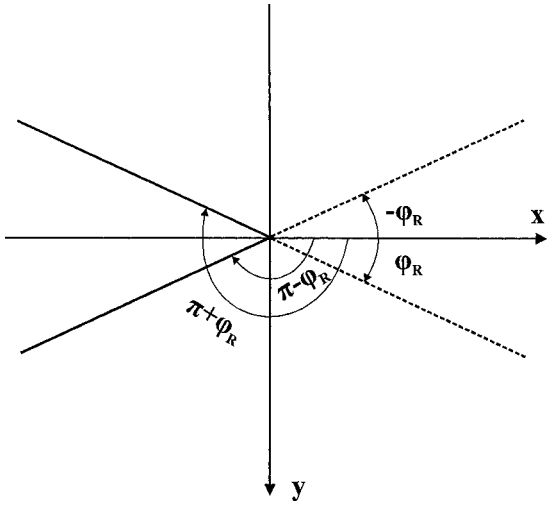

Figure 7. Mach-like Rayleigh wave 'sectors'. Only the trailing Rayleigh wavefronts (continuous lines) are acceptable.

function vanishes (i.e., $R(M_T \sin\varphi) = 0$) and thus the normal displacement $u_z^{(P)}$ is singular. In other words, solution (46), as it stands, predicts *two* Mach-like Rayleigh wave 'sectors'; one ahead of the moving source and the other behind. Nevertheless, as Barber [12] points out only trailing waves of this type should exist. This statement is supported by the radiation condition (see, e.g., [26]) and the observation that the steady-state problem should be viewed as the long-time limit of a *transient* problem, in which the point load (that moves with a super-Rayleigh velocity) is suddenly applied to an initially quiescent half-space, and therefore, one should expect in such a problem the existence of Rayleigh-wave disturbances behind but not ahead of the load (see relative solutions on the transient analogue of the present problem by Payton [31], Gakenheimer and Miklowitz [32], and Bakker et al. [33]). The situation is presented in Figure 7 that depicts the top view of the problem.

We then write the *corrected* solution in this speed range by also taking into account that: (i) the final solution should retain an r^{-1} dependence (this is based on an observation by Willis [34] in general 3D problem with concentrated loads according to which equilibrium demands that the stress field must vary as r^{-2} from the point of application of the force, and therefore, that the displacement field must vary as r^{-1}), (ii) the expression given by the first term of (46) exhibits symmetry w.r.t. both axes x and y, whereas the final solution should retain symmetry only w.r.t. the x-axis, and (iii) the correction added should eliminate the Rayleigh-wave disturbance ahead of the load. The final solution is written as

$$u_z^{(P)}(r,\varphi,z=0) = -\frac{P}{2\mu}\left[\frac{1}{r}F_{11}^{(P)}(M_T\sin\varphi) + \frac{\Omega}{r\sin(\varphi-\varphi_R)} - \frac{\Omega}{r\sin(\varphi+\varphi_R)}\right], \tag{48}$$

where Ω is a yet unknown constant. Following Barber [12], this constant can be determined with the help of the operations described below.

First, we notice from equations (23), (28) and (29b) of the main text and equation (A1) of Appendix A that the function $F_{11}^{(P)}(M_T)$ can be written as

$$F_{11}^{(P)}(M_T) = \frac{(1-M_L^2)^{1/2}[(2-M_T^2)^2 + 4(1-M_L^2)^{1/2}(1-M_T^2)^{1/2}]}{\pi(M_T^2-m_1)(M_T^2-m_2)(M_T^2-m_3)}, \tag{49}$$

where m_j, with $(j = 1, 2, 3)$, are the nontrivial zeroes of the function $K(M_T)$ whose expressions are given in Appendix A. Next, the following definitions are introduced

$$A(M_T) \equiv \frac{4(1-M_L^2)}{\prod_{j=1}^{3}(M_T^2-m_j)}, \qquad B(M_T) \equiv \frac{(2-M_T^2)^2}{\prod_{j=1}^{3}(M_T^2-m_j)}, \tag{50a,b}$$

and the functions (A, B) are subsequently written as sums of partial fractions through the use of the factorization forms provided in equations (A.5) and (A.6) of Appendix A. In view of the above, $F_{11}^{(P)}(M_T)$ in (49) takes the following form, which can directly lead to the determination of the constant Ω through canceling of the terms that generate the *undesirable* Rayleigh-wave singularities mentioned before

$$\begin{aligned} F_{11}^{(P)}(M_T \sin\varphi) \;=\; & \frac{1}{\pi}\sum_{j=1}^{3}\frac{A_j(1-M_T^2\sin^2\varphi)^{1/2}}{(M_T^2\sin^2\varphi - m_j)} \\ & + \frac{1}{\pi}\sum_{j=1}^{3}\frac{B_j(1-M_L^2\sin^2\varphi)^{1/2}}{(M_T^2\sin^2\varphi - m_j)}, \end{aligned} \tag{51}$$

where the new constants (A_j, B_j), with $(j = 1, 2, 3)$, are given in equations (A.9) and (A.10) of Appendix A and solely depend upon the Poisson's ratio of the material. Finally, in view of (51) and the definition of φ_R, solution (48) becomes

$$\begin{aligned} u_z^{(P)}(r,\varphi,z=0) \;=\; & -\frac{P}{2\mu\pi r}\left[\sum_{j=1}^{3}\frac{A_j(1-M_T^2\sin^2\varphi)^{1/2}}{(M_T^2\sin^2\varphi - m_j)}\right. \\ & \left. + \sum_{j=1}^{3}\frac{B_j(1-M_L^2\sin^2\varphi)^{1/2}}{(M_T^2\sin^2\varphi - m_j)} + \frac{2\Omega m_1^{1/2} M_T\cos\varphi}{M_T^2\sin^2\varphi - m_1}\right]. \end{aligned} \tag{52}$$

From the above form, it is clear now that Ω should be chosen so that the terms corresponding to the case $j = 1$ to be canceled along the Rayleigh wave singularities ahead of the load, that is for $\varphi = \pm\varphi_R$. In this way, by solving the equation

$$\begin{aligned} & A_1\left(1-M_T^2\sin^2\varphi_R\right)^{1/2} + B_1\left(1-m^{-2}M_T^2\sin^2\varphi_R\right)^{1/2} \\ & \quad + 2\Omega m_1^{1/2} M_T\cos\varphi_R = 0, \end{aligned} \tag{53}$$

we obtain the appropriate value of Ω as

$$\Omega = -\frac{M_T(1-m^{-2}m_1)^{1/2}[(2-m_1)^2+4(1-m_1)^{1/2}(1-m^{-2}m_1)^{1/2}]}{2m_1^{1/2}M_T(M_T^2-m_1)^{1/2}(m_1-m_2)(m_1-m_3)}, \tag{54}$$

and, further, from (52) the final solution in the range $V_R < V < V_T$

$$\begin{aligned} u_z^{(P)}&(r,\varphi,z=0) \\ &= -\frac{P}{2\mu\pi r}\Bigg[\pi F_{11}^{(P)}(M_T\sin\varphi) \\ &\quad - \frac{M_T\cos\varphi\cdot(1-m^{-2}m_1)^{1/2}[(2-m_1)^2+4(1-m_1)^{1/2}(1-m^{-2}m_1)^{1/2}]}{(M_T^2\sin^2\varphi-m_1)(M_T^2-m_1)^{1/2}(m_1-m_2)(m_1-m_3)}\Bigg] \end{aligned} \tag{55}$$

6.1.3. *Transonic Range* ($V_T < V < V_L$)

In this case, both terms in the RHS of (46) contribute. Also, the functions $F_1^{(P)}(M_T\sin\varphi)$ and $F_2^{(P)}(M_T\sin\varphi)$ because of (23), (24), (49), (50a,b) and (A.1) are written as

$$\begin{aligned} \pi F_1^{(P)}(M_T\sin\varphi) &= A(M_T\sin\varphi)\big(1-M_T^2\sin^2\varphi\big)^{1/2}H\big(V_T-V|\sin\varphi|\big) + \\ &\quad + B(M_T\sin\varphi)\big(1-M_L^2\sin^2\varphi\big)^{1/2}, \end{aligned} \tag{56a}$$

$$\begin{aligned} F_2^{(P)}\big(M_T(1-\zeta^2)^{1/2}\big) &= A\big(M_T(1-\zeta^2)^{1/2}\big)\big(M_T^2-M_T^2\zeta^2-1\big)^{1/2} \\ &\quad \times H\big(V(1-\zeta^2)^{1/2}-V_T\big). \end{aligned} \tag{56b}$$

Substituting then (56) in (46) provides

$$\begin{aligned} u_z^{(P)}&(r,\varphi,z=0) \\ &= -\frac{P}{2\mu\pi r}\big[A(M_T\sin\varphi)\cdot\big(1-M_T^2\sin^2\varphi\big)^{1/2}H\big(V_T-V|\sin\varphi|\big) \\ &\quad + B(M_T\sin\varphi)(1-M_L^2\sin^2\varphi)^{1/2}\big] - \frac{P\cos\varphi}{\mu\pi^2 r} \\ &\quad \times \int_0^{[1-(1/M_T^2)]^{1/2}} A\big(M_T(1-\zeta^2)^{1/2}\big)\big(M_T^2-M_T^2\zeta^2-1\big)^{1/2} \\ &\quad \times \mathbf{PF}\left(\frac{1}{\cos^2\varphi-\zeta^2}\right)\mathrm{d}\zeta. \end{aligned} \tag{57}$$

Here, an analysis of the integral in the RHS of (57) should be provided. This reveals, in fact, that the integral is a well-defined Cauchy *principal-value* integral. Considering (50a), the following points are noted about the integral:

(i) the analysis in Appendix A shows that the zero of the term $M_T^2-m_1-M_T^2\zeta^2$ lies outside the integration interval,

(ii) the terms $M_T^2 - m_j - M_T^2\zeta^2$, with $(j = 2, 3)$, do not have zeros in this velocity regime because it is valid that $m_3 > m_2 > M_T^2$ – see Appendix A,

(iii) along those angles φ defined by $\cos^2\varphi = 0$, the integral diverges but thanks to its coefficient $\cos\varphi$ the integral term in (57) eventually vanishes, and

(iv) along those angles φ defined by $\cos^2\varphi = [1 - (1/M_T^2)]$ (the angles correspond to the shear Mach wavefronts), the integrand exhibits an integrable behavior varying as $([1 - (1/M_T^2)]^{1/2} - \zeta)^{-1/2}$. Therefore, the integrand in (57) exhibits only one pole at $\zeta = |\cos\varphi|$, and the associated integral is a Cauchy *principal-value* integral contributing *no* singularity in the displacement.

The only singularity in (57) is the Rayleigh-type singularity stemming from the first term of this expression. This term also indicates the existence of the pertinent shear Mach wavefronts since it contains the Heaviside step function $H(V_T - V|\sin\varphi|)$. One can work now as in the previous super-Rayleigh/subsonic case to eliminate the singularity ahead of the load and, finally, the following expression is found for the surface vertical displacement $u_z^{(P)}$ due to the vertical load P in the transonic range

$$
\begin{aligned}
&u_z^{(P)}(r, \varphi, z = 0) \\
&\quad = -\frac{P}{2\mu\pi r}\Bigg[A(M_T \sin\varphi)\big(1 - M_T^2 \sin^2\varphi\big)^{1/2} H\big(V_T - V|\sin\varphi|\big) \\
&\qquad + B(M_T \sin\varphi)\big(1 - M_L^2 \sin^2\varphi\big)^{1/2} \\
&\qquad - \frac{M_T \cos\varphi (1 - m^{-2}m_1)^{1/2}[(2 - m_1)^2 + 4(1 - m_1)^{1/2}(1 - m^{-2}m_1)^{1/2}]}{(M_T^2 \sin^2\varphi - m_1)(M_T^2 - m_1)^{1/2}(m_1 - m_2)(m_1 - m_3)} \Bigg] \\
&\qquad - \frac{P \cdot \cos\varphi}{\mu\pi^2 r} \int_0^{[1-(1/M_T^2)]^{1/2}} A\big(M_T(1 - \zeta^2)^{1/2}\big)\big(M_T^2 - M_T^2\zeta^2 - 1\big)^{1/2} \\
&\qquad \times \mathbf{PF}\left(\frac{1}{\cos^2\varphi - \zeta^2}\right) \mathrm{d}\zeta. \qquad (58)
\end{aligned}
$$

The Cauchy *principal-value* integral in (58) as well as all integrals in the other results below was evaluated by using the *numerical* algorithms of the program MATHEMATICA™ – version 3.0. Numerical results in the form of graphs are presented in Section 9.

6.1.4. *Supersonic Range* $(V_L < V)$

Working again on the basic result of equation (46), we get the expression

$$
\begin{aligned}
&u_z^{(P)}(r, \varphi, z = 0) \\
&\quad = -\frac{P}{2\mu\pi r}\big[A(M_T \sin\varphi)\big(1 - M_T^2 \sin^2\varphi\big)^{1/2} H\big(V_T - V|\sin\varphi|\big) \\
&\qquad + B(M_T \sin\varphi)\big(1 - M_L^2 \sin^2\varphi\big)^{1/2} H\big(V_L - V|\sin\varphi|\big)\big]
\end{aligned}
$$

$$
\begin{aligned}
&- \frac{P \cdot \cos\varphi}{\mu\pi^2 r} \int_0^{[1-(1/M_{\mathrm{L}}^2)]^{1/2}} \left[A\left(M_{\mathrm{T}}(1-\zeta^2)^{1/2}\right)\left(M_{\mathrm{T}}^2 - M_{\mathrm{T}}^2\zeta^2 - 1\right)^{1/2}\right. \\
&\left. + B\left(M_{\mathrm{T}}(1-\zeta^2)^{1/2}\right)\left(M_{\mathrm{L}}^2 - M_{\mathrm{L}}^2\zeta^2 - 1\right)^{1/2}\right] \mathbf{PF}\left(\frac{1}{\cos^2\varphi - \zeta^2}\right) \mathrm{d}\zeta \\
&- \frac{P \cdot \cos\varphi}{\mu\pi^2 r} \int_{[1-(1/M_{\mathrm{L}}^2)]^{1/2}}^{[1-(1/M_{\mathrm{T}}^2)]^{1/2}} A\left(M_{\mathrm{T}}(1-\zeta^2)^{1/2}\right)\left(M_{\mathrm{T}}^2 - M_{\mathrm{T}}^2\zeta^2 - 1\right)^{1/2} \\
&\times \mathbf{PF}\left(\frac{1}{\cos^2\varphi - \zeta^2}\right) \mathrm{d}\zeta. \qquad (59)
\end{aligned}
$$

The first term in the RHS of (59) is particularly simple and instructive since it clearly exhibits the appearance of the longitudinal and shear Mach wavefronts. These wavefronts stem from the two Heaviside step functions. However, the integrals require a careful analysis.

Regarding the first integral, one may notice the following:

(i) Relation (27b) and Appendix A indicate that $m_1 < m^2$ and, therefore, the term $M_{\mathrm{T}}^2 - m_1 - M_{\mathrm{T}}^2\zeta^2$ has no zeros inside the integration interval.

(ii) The analysis in Appendix A suggests that the zeros m_2 and m_3 of the function $K(M_{\mathrm{T}})$ are real numbers when the Poisson ratio ν satisfies the inequalities $0 < \nu \leqslant \nu_0$, where $\nu_0 = 0.2630820648\ldots$. In addition, in the supersonic regime, the inequalities $m_2 < M_{\mathrm{T}}^2$ and/or $m_3 < M_{\mathrm{T}}^2$ may be satisfied and, accordingly, the zeros of the terms $M_{\mathrm{T}}^2 - m_j - M_{\mathrm{T}}^2\zeta^2$, with $(j = 2, 3)$, may lie within the integration interval. However, it can be shown that these points correspond to removable singularities.

(iii) Along the lines $\cos^2\varphi = [1 - (1/M_{\mathrm{L}}^2)]$, which correspond to the longitudinal Mach wavefronts, the integrand remains integrable since it behaves like $([1 - (1/M_{\mathrm{L}}^2)]^{1/2} - \zeta)^{-1/2}$ at the upper integration limit.

Regarding now the second integral, one may notice that: (i) The zeros of the term $M_{\mathrm{T}}^2 - m_1 - M_{\mathrm{T}}^2\zeta^2$ lie outside the integration interval, since (A.3) indicates that $m_1 < 1$. (ii) The zeros of the terms $M_{\mathrm{T}}^2 - m_j - M_{\mathrm{T}}^2\zeta^2$, with $(j = 2, 3)$, lie outside the integration interval. (iii) Along the shear Mach wavefront (upper integration limit), the integrand behaves like an inverse square root and is, therefore, integrable. Along the longitudinal Mach wavefront, the integrand is smooth. Finally, one may observe, that in the two integrands of (59) only one pole appears at the point $\zeta = |\cos\varphi|$. Therefore, the integrals in (59) can be evaluated in the Cauchy *principal-value* sense without any difficulty.

In view of the above observations, we may conclude that there are no other singularities for the surface vertical displacement $u_z^{(P)}(r, \varphi, z = 0)$ except for the Rayleigh-type singularity exhibited by the first (non-integral) term of (59). This singularity is due to the terms $A(M_{\mathrm{T}}\sin\varphi)$ and $B(M_{\mathrm{T}}\sin\varphi)$. Following the same procedure as in the previous cases of a super-Rayleigh/subsonic speed and a transonic speed of the moving load, the complete solution for the present supersonic case is obtained as

$$
\begin{aligned}
&u_z^{(P)}(r,\varphi,z=0)\\
&\quad=-\frac{P}{2\mu\pi r}\Bigg[A(M_{\mathrm{T}}\sin\varphi)\big(1-M_{\mathrm{T}}^2\sin^2\varphi\big)^{1/2}H\big(V_{\mathrm{T}}-V|\sin\varphi|\big)\\
&\qquad+B(M_{\mathrm{T}}\sin\varphi)\big(1-M_{\mathrm{L}}^2\sin^2\varphi\big)^{1/2}H(V_{\mathrm{L}}-V|\sin\varphi|)\\
&\qquad-\frac{M_{\mathrm{T}}\cos\varphi\cdot(1-m^{-2}m_1)^{1/2}[(2-m_1)^2+4(1-m_1)^{1/2}(1-m^{-2}m_1)^{1/2}]}{(M_{\mathrm{T}}^2\sin^2\varphi-m_1)(M_{\mathrm{T}}^2-m_1)^{1/2}(m_1-m_2)(m_1-m_3)}\Bigg]\\
&\qquad-\frac{P\cdot\cos\varphi}{\mu\pi^2 r}\int_0^{[1-(1/M_{\mathrm{L}}^2)]^{1/2}}B\big(M_{\mathrm{T}}(1-\zeta^2)^{1/2}\big)\big(M_{\mathrm{L}}^2-M_{\mathrm{L}}^2\zeta^2-1\big)^{1/2}\\
&\qquad\times\mathbf{PF}\bigg(\frac{1}{\cos^2\varphi-\zeta^2}\bigg)\,\mathrm{d}\zeta-\frac{P\cdot\cos\varphi}{\mu\pi^2 r}\int_0^{[1-(1/M_{\mathrm{L}}^2)]^{1/2}}A\big(M_{\mathrm{T}}(1-\zeta^2)^{1/2}\big)\\
&\qquad\times\big(M_{\mathrm{T}}^2-M_{\mathrm{T}}^2\zeta^2-1\big)^{1/2}\mathbf{PF}\bigg(\frac{1}{\cos^2\varphi-\zeta^2}\bigg)\,\mathrm{d}\zeta-\frac{P\cdot\cos\varphi}{\mu\pi^2 r}\\
&\qquad\times\int_{[1-(1/M_{\mathrm{T}}^2)]^{1/2}}^{[1-(1/M_{\mathrm{L}}^2)]^{1/2}}A\big(M_{\mathrm{T}}(1-\zeta^2)^{1/2}\big)\big(M_{\mathrm{T}}^2-M_{\mathrm{T}}^2\zeta^2-1\big)^{1/2}\mathbf{PF}\bigg(\frac{1}{\cos^2\varphi-\zeta^2}\bigg)\,\mathrm{d}\zeta.
\end{aligned}
\tag{60}
$$

This concludes the presentation of results for the surface vertical displacement $u_z^{(P)}$ due to the vertical load P. Our results agree with respective results by Lansing [6] and Barber [12] in the entire speed range, and with the sub-Rayleigh results of Eason [11] (notice that Eason restricted himself in a sub-Rayleigh analysis of the problem only). Finally, as noted in the Introduction, the integrals in (58) and (60) were evaluated in closed analytical forms by Barber [12]. We chose, however, to give the results in integral forms that are amenable to numerical evaluation by MATHEMATICA™ because in all other cases considered here closed analytical forms are impossible to be obtained.

6.2. VERTICAL DISPLACEMENT $u_z^{(S)}$ DUE TO THE TANGENTIAL LOAD S

Operating with the inverse Radon transform on (20) and (22a) (i.e., on the solution of the first auxiliary problem involving the tangential load that is in the direction of motion) and proceeding in an similar manner as in the previous case of the vertical load, we obtain

$$
\begin{aligned}
u_z^{(S)}(r,\varphi,z=0)\;=\;&-\frac{S}{2\mu r}F_1^{(S)}(M_{\mathrm{T}}\sin\varphi)\cdot|\sin\varphi|-\frac{S\cos\varphi}{\mu\pi^2 r}\\
&\times\int_0^1 F_2^{(S)}\big(M_{\mathrm{T}}(1-\zeta^2)^{1/2}\big)(1-\zeta^2)^{1/2}\,\mathbf{PF}\bigg(\frac{1}{\cos^2\varphi-\zeta^2}\bigg)\,\mathrm{d}\zeta.
\end{aligned}
\tag{61}
$$

Again, from this basic result, particular results will be obtained below for the entire speed regime, i.e., for $0 < V < V_R$, $V_R < V < V_T$, $V_T < V < V_L$ and $V_L < V$. These results will depend of course upon the particular forms of the functions $F_1^{(S)}(\cdot)$ and $F_2^{(S)}(\cdot)$ in each speed range. Finally, equation (62) clearly exhibits the required symmetry of $u_z^{(S)}$ w.r.t. the x-axis.

6.2.1. *Sub-Rayleigh Range* ($0 < V < V_R$)

In this range, only the integral in (62) contributes since $F_{11}^{(S)}(M_T \sin\varphi) = 0$ for all angles φ. Thus, the result is found to be

$$\begin{aligned} u_z^{(S)} \;=\; & -\frac{S\cdot\cos\varphi}{\mu\pi^2 r}\int_0^1 \Big[C\big(M_T(1-\zeta^2)^{1/2}\big) + D\big(M_T(1-\zeta^2)^{1/2}\big) \\ & \times \big(1 - M_T^2 + M_T^2\zeta^2\big)^{1/2}\big(1 - M_L^2 + M_L^2\zeta^2\big)^{1/2}\Big]\big(1-\zeta^2\big)^{1/2} \\ & \times \mathbf{PF}\left(\frac{1}{\cos^2\varphi - \zeta^2}\right)\mathrm{d}\zeta, \end{aligned} \tag{62}$$

where

$$\begin{aligned} C(M_T) &= \frac{(8m^{-2}-4) + (6-8m^{-2})M_T^2 - M_T^4}{\prod_{j=1}^3 (M_T^2 - m_j)}, \\ D(M_T) &= \frac{2(2-M_T^2)}{\prod_{j=1}^3 (M_T^2 - m_j)}. \end{aligned} \tag{63a,b}$$

This result is in agreement with the respective result in the study by Eason [11].

6.2.2. *Super-Rayleigh Subsonic Range* ($V_R < V < V_T$)

The displacement $u_z^{(S)}$ is still given by (62). However, in this case there are two poles at the points $\zeta = [1 - (m_1/M_T^2)]^{1/2}$ and $\zeta = |\cos\varphi|$. No additional poles arise since, in view of (A.4), the terms $M_T^2 - m_j - M_T^2\zeta^2$, with $(j = 2, 3)$, exhibit no zeros. One may obtain

$$\begin{aligned} u_z^{(S)} \;=\; & -\frac{S\cdot\cos\varphi}{\mu\pi^2 r}\int_0^1 \Big[C^*\big(M_T(1-\zeta^2)^{1/2}\big) \\ & + D^*\big(M_T(1-\zeta^2)^{1/2}\big)\big(1 - M_T^2 + M_T^2\zeta^2\big)^{1/2}\big(1 - M_L^2 + M_L^2\zeta^2\big)^{1/2}\Big] \\ & \times \big(1-\zeta^2\big)^{1/2}\,\mathbf{PF}\left(\frac{1}{M_T^2 - m_1 - M_T^2\zeta^2}\right)\mathbf{PF}\left(\frac{1}{\cos^2\varphi - \zeta^2}\right)\mathrm{d}\zeta, \end{aligned} \tag{64}$$

where

$$C^*(M_T) = C(M_T)\big(M_T^2 - m_1\big), \qquad D^*(M_T) = D(M_T)\big(M_T^2 - m_1\big). \tag{65a,b}$$

As long as the two poles in the integrand of (64) do not coincide, no difficulty arises for the evaluation of the integral even by the use of MATHEMATICA™.

The two poles coincide when $\cos^2\varphi = [1 - (m_1/M_{\mathrm{T}}^2)]$, which are directions corresponding to the Rayleigh Mach wavefronts. A double pole then arises and the solution takes the form

$$\begin{aligned} u_z^{(S)} \;=\; & -\frac{S\cos\varphi}{\mu\pi^2 r}\int_0^1 \Big[C^*\big(M_{\mathrm{T}}(1-\zeta^2)^{1/2}\big) \\ & + D^*\big(M_{\mathrm{T}}(1-\zeta^2)^{1/2}\big)\big(1-M_{\mathrm{T}}^2+M_{\mathrm{T}}^2\zeta^2\big)^{1/2}\big(1-M_{\mathrm{L}}^2+M_{\mathrm{L}}^2\zeta^2\big)^{1/2}\Big] \\ & \times (1-\zeta^2)^{1/2}\frac{1}{M_{\mathrm{T}}^2}\cdot\mathbf{PF}\bigg(\frac{1}{([1-(m_1/M_{\mathrm{T}}^2)]-\zeta^2)^2}\bigg)\,\mathrm{d}\zeta, \end{aligned} \tag{66}$$

where $\mathbf{PF}(\cdot)$ denotes now the *finite-part* (or *second-order* principal-part) pseudo-function or distribution (see, e.g., [17, 19]). In other words, the integral in (66) should be interpreted as a Hadamard *finite-part* integral [19]. This means that

$$\big\langle \mathbf{PF}(1/x^2), \phi\big\rangle = \lim_{\varepsilon\to 0}\int_{|x|\geqslant\varepsilon}\frac{\phi(x)-\phi(0)}{x^2}\,\mathrm{d}x,$$

where $\langle\cdot,\cdot\rangle$ denotes the inner product of distributions, ε is a real and positive number, and ϕ is a test function. Equivalently, the second-order principal-part pseudo-function is the negative of the derivative of the principal-value pseudo-function, i.e., $\mathbf{PF}(1/x^2) = -\mathbf{PF}'(1/x)$. In view of the above, the vertical displacement $u_z^{(S)}$ given by (66) remains bounded even along the Rayleigh wavefronts.

6.2.3. *Transonic Range* ($V_{\mathrm{T}} < V < V_{\mathrm{L}}$)

Working as in the latter case, the combination of equations (25), (26), (61), (63) and (65) provides the result

$$\begin{aligned} & u_z^{(S)}(r,\varphi,z=0) \\ & = \frac{S|\sin\varphi|}{2\mu\pi r}D(M_{\mathrm{T}}\sin\varphi)\big(1-M_{\mathrm{L}}^2\sin^2\varphi\big)^{1/2}\big(M_{\mathrm{T}}^2\sin^2\varphi-1\big)^{1/2} \\ & \quad\times H\bigg(|\sin\varphi|-\frac{1}{M_{\mathrm{T}}}\bigg) - \frac{S\cdot\cos\varphi}{\mu\pi^2 r}\bigg[\int_0^1 C^*\big(M_{\mathrm{T}}(1-\zeta^2)^{1/2}\big)\cdot\big(1-\zeta^2\big)^{1/2} \\ & \quad\times\mathbf{PF}\bigg(\frac{1}{M_{\mathrm{T}}^2-m_1-M_{\mathrm{T}}^2\zeta^2}\bigg)\cdot\mathbf{PF}\bigg(\frac{1}{\cos^2\varphi-\zeta^2}\bigg)\,\mathrm{d}\zeta \\ & \quad+\int_{[1-(1/M_{\mathrm{T}}^2)]^{1/2}}^1 D^*\big(M_{\mathrm{T}}(1-\zeta^2)^{1/2}\big)\big(1-M_{\mathrm{T}}^2+M_{\mathrm{T}}^2\zeta^2\big)^{1/2} \\ & \quad\times\big(1-M_{\mathrm{L}}^2+M_{\mathrm{L}}^2\zeta^2\big)^{1/2} \\ & \quad\times\big(1-\zeta^2\big)^{1/2}\mathbf{PF}\bigg(\frac{1}{M_{\mathrm{T}}^2-m_1-M_{\mathrm{T}}^2\zeta^2}\bigg)\mathbf{PF}\bigg(\frac{1}{\cos^2\varphi-\zeta^2}\bigg)\,\mathrm{d}\zeta\bigg]. \end{aligned} \tag{67}$$

The first integrand in (67) exhibits poles at the points $\zeta = [1-(m_1/M_{\mathrm{T}}^2)]^{1/2}$ and $\zeta = |\cos\varphi|$, whereas the second integrand exhibits a pole at $\zeta = [1-(m_1/M_{\mathrm{T}}^2)]^{1/2}$

in any case and at $\zeta = |\cos\varphi|$ only if $\cos^2\varphi > [1 - (1/M_T^2)]$. Both integrals are evaluated as Cauchy *principal-value* integrals and are amenable to a direct numerical treatment.

6.2.4. *Supersonic Range* ($V_L < V$)

Here, equations (25), (26), (61) and (63) yield

$$\begin{aligned} u_z^{(S)}(r,\varphi,z=0) &= \frac{S|\sin\varphi|}{2\mu\pi r}\cdot D(M_T\sin\varphi)\big(1-M_L^2\sin^2\varphi\big)^{1/2}\big(M_T^2\sin^2\varphi-1\big)^{1/2} \\ &\quad\times\left[H\left(|\sin\varphi|-\frac{1}{M_T}\right)-H\left(|\sin\varphi|-\frac{1}{M_L}\right)\right] \\ &\quad-\frac{S\cos\varphi}{\mu\pi^2 r}\Bigg[\int_0^1 C\big(M_T(1-\zeta^2)^{1/2}\big)\big(1-\zeta^2\big)^{1/2}\,\mathbf{PF}\left(\frac{1}{\cos^2\varphi-\zeta^2}\right)\mathrm{d}\zeta \\ &\quad-\int_0^{[1-(1/M_L^2)]^{1/2}} D\big(M_T(1-\zeta^2)^{1/2}\big)\big(M_T^2-M_T^2\zeta^2-1\big)^{1/2} \\ &\quad\times\big(M_L^2-M_L^2\zeta^2-1\big)^{1/2}\big(1-\zeta^2\big)^{1/2}\,\mathbf{PF}\left(\frac{1}{\cos^2\varphi-\zeta^2}\right)\mathrm{d}\zeta\Bigg] \\ &\quad+\int_{[1-(1/M_T^2)]^{1/2}}^1 D\big(M_T(1-\zeta^2)^{1/2}\big)\big(1-M_T^2+M_T^2\zeta^2\big)^{1/2} \\ &\quad\times\big(1-M_L^2+M_L^2\zeta^2\big)^{1/2}(1-\zeta^2)^{1/2}\,\mathbf{PF}\left(\frac{1}{\cos^2\varphi-\zeta^2}\right)\mathrm{d}\zeta\Bigg]. \end{aligned} \tag{68}$$

In general, the numerical evaluation of (68) does not pose particular difficulties, except in the case of Poisson's ratios in the range $\nu \leqslant \nu_0$. This is due to the fact that the zeros of the function $K(M_T)$ are real and, therefore, the integrands along the integration intervals [0, 1] and [0, $[1 - (1/M_L^2)]^{1/2}$] may exhibit more than two distinct poles. Since the program MATHEMATICA™ cannot numerically evaluate an integral with an integrand containing more than two pole singularities, we reduce these integrals to forms that contain at most two pole singularities. Indeed, this is accomplished by writing the terms $C(M_T(1-\zeta^2)^{1/2})$ and $D(M_T(1-\zeta^2)^{1/2})$ as partial fractions according to equations (A.7), (A.8), (A.11) and (A.12) of Appendix A. In this way, the first two integrals in (68), say I_1 and I_2, are expressed by the following forms that now permit numerical evaluation by MATHEMATICA™

$$\begin{aligned} I_1 &= \sum_{j=1}^{3} C_j \int_0^1 \mathbf{PF}\left(\frac{1}{M_T^2-m_j-M_T^2\zeta^2}\right)\big(1-\zeta^2\big)^{1/2} \\ &\quad\times\mathbf{PF}\left(\frac{1}{\cos^2\varphi-\zeta^2}\right)\mathrm{d}\zeta, \end{aligned} \tag{69}$$

$$I_2 = \sum_{j=1}^{3} D_j \int_0^{[1-(1/M_{\mathrm{L}}^2)]^{1/2}} \mathbf{PF}\left(\frac{1}{M_{\mathrm{T}}^2 - m_j - M_{\mathrm{T}}^2\zeta^2}\right)\left(M_{\mathrm{T}}^2 - M_{\mathrm{T}}^2\zeta^2 - 1\right)^{1/2} \times \left(M_{\mathrm{L}}^2 - M_{\mathrm{L}}^2\zeta^2 - 1\right)^{1/2}\left(1-\zeta^2\right)^{1/2} \mathbf{PF}\left(\frac{1}{\cos^2\varphi - \zeta^2}\right) \mathrm{d}\zeta, \tag{70}$$

where the constants (C_j, D_j) are given in Appendix A.

6.3. VERTICAL DISPLACEMENT $u_z^{(T)}$ DUE TO THE TANGENTIAL LOAD T

In this case, we operate with (10) on (20) and (22b) and obtain the result

$$\begin{aligned} u_z^{(T)}&(r,\varphi,z=0) \\ &= -\frac{T}{4\mu}\left\{\int_0^{2\pi}\left[\sin\omega\cdot\operatorname{sgn}(\sin\omega)\cdot F_1^{(S)}(M_{\mathrm{T}}\cos\omega)\delta(r\cos(\omega-\varphi))\right]\mathrm{d}\omega \right. \\ &\left. + \int_0^{2\pi}\left[\operatorname{sgn}(\cos\omega)\cdot F_2^{(S)}(M_{\mathrm{T}}\cos\omega)\,\mathbf{PF}\left(\frac{1}{\pi^2 r\cdot\cos(\omega-\varphi)}\right)\right]\mathrm{d}\omega\right\}. \end{aligned} \tag{71}$$

Further, using properties of the Dirac delta distribution and performing the monotonic change of variable $\zeta = \sin\omega$, we get

$$\begin{aligned} u_z^{(T)}(r,\varphi,z=0) &= -\frac{T}{2\mu r}F_1^{(S)}(M_{\mathrm{T}}\sin\varphi)\cdot|\cos\varphi| \\ &\quad - \frac{T\cdot\cos\varphi}{\mu\pi^2 r}\int_0^1 F_2^{(S)}\left(M_{\mathrm{T}}(1-\zeta^2)^{1/2}\right)\cdot\zeta \\ &\quad \times \mathbf{PF}\left(\frac{1}{\cos^2\varphi-\zeta^2}\right)\mathrm{d}\zeta. \end{aligned} \tag{72}$$

From the above general result now, particular results are derived for the sub-Rayleigh and super-Rayleigh subsonic range. No details are given, however, since (72) strongly resembles (61), which was analyzed in detail before.

6.3.1. *Sub-Rayleigh Range* $(0 < V < V_{\mathrm{R}})$

In this range, only the integral in (72) contributes since $F_{11}^{(S)}(M_{\mathrm{T}}\sin\varphi) = 0$ for all angles φ. Therefore, we have

$$\begin{aligned} u_z^{(T)} &= -\frac{T\cdot\cos\varphi}{\mu\pi^2 r}\int_0^1 \left[C\left(M_{\mathrm{T}}(1-\zeta^2)^{1/2}\right)\right. \\ &\quad \left. + D\left(M_{\mathrm{T}}(1-\zeta^2)^{1/2}\right)\left(1-M_{\mathrm{T}}^2+M_{\mathrm{T}}^2\zeta^2\right)^{1/2}\left(1-M_{\mathrm{L}}^2+M_{\mathrm{L}}^2\zeta^2\right)^{1/2}\right] \\ &\quad \times\zeta\cdot\mathbf{PF}\left(\frac{1}{\cos^2\varphi-\zeta^2}\right)\mathrm{d}\zeta, \end{aligned} \tag{73}$$

where $C(M_{\mathrm{T}})$ and $D(M_{\mathrm{T}})$ are given by equations (63).

6.3.2. *Super-Rayleigh Subsonic Range* ($V_R < V < V_T$)

$$u_z^{(T)} = -\frac{T\cdot\cos\varphi}{\mu\pi^2 r}\int_0^1 \Big[C^*\big(M_T(1-\zeta^2)^{1/2}\big) + D^*\big(M_T(1-\zeta^2)^{1/2}\big)\big(1-M_T^2+M_T^2\zeta^2\big)^{1/2}\big(1-M_L^2+M_L^2\zeta^2\big)^{1/2}\Big] \times \zeta\cdot\mathbf{PF}\left(\frac{1}{M_T^2-m_1-M_T^2\zeta^2}\right)\mathbf{PF}\left(\frac{1}{\cos^2\varphi-\zeta^2}\right)\mathrm{d}\zeta, \tag{74}$$

where $C^*(M_T)$ and $D^*(M_T)$ are given by equations (65).

7. Additional Results: Tangential Displacements

In general, the tangential displacements (u_x, u_y) can be found by operating with the inverse Radon transform on the transformed displacements $(\tilde{u}_x, \tilde{u}_y)$. The latter expressions result, of course, from (38) and the expressions for $(\tilde{u}_q, \tilde{u}_s)$. Then, the components (u_r, u_φ) in the cylindrical polar coordinate system may readily be obtained through the coordinate transformation (39).

As before, the displacements will be obtained separately for the cases of vertical and tangential loading. Also, in accordance with the results provided for $\tilde{u}_q(q, \omega, z = 0)$ in Section 4, we will avoid below the less practical case of the T load and consider only the loading (P, S).

7.1. TANGENTIAL DISPLACEMENTS DUE TO THE VERTICAL LOAD P

In this case, the solution to the first auxiliary problem is given by (31) and (33), whereas the solution to the second auxiliary problem is $\tilde{u}_s(q, \omega, z = 0) = 0$ since the boundary condition associated with (14) is $\tilde{\sigma}_{zs}(q, \omega, z = 0) = 0$. Accordingly, the following Radon transformed solutions are obtained

$$\tilde{u}_x^{(P)}(q, \omega, z = 0) = -\frac{P\cdot\operatorname{sgn}(\cos\omega)\cdot\cos\omega}{2\mu}G^{(P)}(M_T\cos\omega) \times \operatorname{sgn}\big(\operatorname{sgn}(\cos\omega)\cdot q\big), \tag{75}$$

$$\tilde{u}_y^{(P)}(q, \omega, z = 0) = -\frac{P\cdot\operatorname{sgn}(\cos\omega)\cdot\sin\omega}{2\mu}G^{(P)}(M_T\cos\omega) \times \operatorname{sgn}\big(\operatorname{sgn}(\cos\omega)\cdot q\big), \tag{76}$$

and further from (10), (40), (44) and by the monotonic change of variable $\zeta = \sin\omega$, the tangential (horizontal) displacements are obtained as

$$u_x^{(P)}(r, \varphi, z = 0) = -\frac{P\cos\varphi}{\mu\pi^2 r}\int_0^1 G^{(P)}\big(M_T(1-\zeta^2)^{1/2}\big)\big(1-\zeta^2\big)^{1/2} \times \mathbf{PF}\left(\frac{1}{\cos^2\varphi-\zeta^2}\right)\mathrm{d}\zeta, \tag{77}$$

$$u_y^{(P)}(r,\varphi,z=0) = \frac{P\sin\varphi}{\mu\pi^2 r}\int_0^1 G^{(P)}\big(M_{\mathrm{T}}(1-\zeta^2)^{1/2}\big)\frac{\zeta^2}{(1-\zeta^2)^{1/2}} \times \mathbf{PF}\left(\frac{1}{\cos^2\varphi-\zeta^2}\right)\mathrm{d}\zeta, \tag{78}$$

where

$$G^{(P)}\big(M_{\mathrm{T}}(1-\zeta^2)^{1/2}\big) = -C\big(M_{\mathrm{T}}(1-\zeta^2)^{1/2}\big) - D\big(M_{\mathrm{T}}(1-\zeta^2)^{1/2}\big) \times \big(1-M_{\mathrm{T}}^2+M_{\mathrm{T}}^2\zeta^2\big)^{1/2}\big(1-M_{\mathrm{L}}^2+M_{\mathrm{L}}^2\zeta^2\big)^{1/2}. \tag{79}$$

One may observe now that the expression for $u_x^{(P)}$ coincides with that for $u_z^{(S)}$, the latter being given by (62). This is not surprising in view of the dynamic version of the Betti–Rayleigh reciprocal theorem. Notice also that an opposite sign in the two expressions is due to the different direction of the loads w.r.t. the corresponding displacements. In view of this, the previous analysis concerning $u_z^{(S)}$ in the subsonic range is carried over the case of $u_x^{(P)}$ too. An inspection also on (77) and (78) reveals that both $u_x^{(P)}$ and $u_y^{(P)}$ do not exhibit Rayleigh–Mach wavefronts. Equations (77) and (78) hold in the entire subsonic velocity range.

Finally, from (39), (77) and (78), the displacement components in a system of cylindrical polar coordinates (r,φ,z) (see Figure 6) are found to be

$$u_r^{(P)}(r,\varphi,z=0) = -\frac{P}{\mu\pi^2 r}\int_0^1 G^{(P)}\big(M_{\mathrm{T}}(1-\zeta^2)^{1/2}\big)\frac{1}{(1-\zeta^2)^{1/2}}\,\mathrm{d}\zeta, \tag{80}$$

$$u_\varphi^{(P)}(r,\varphi,z=0) = \frac{P\cos\varphi\cdot\sin\varphi}{\mu\pi^2 r}\int_0^1 G^{(P)}\big(M_{\mathrm{T}}(1-\zeta^2)^{1/2}\big) \times \frac{1}{(1-\zeta^2)^{1/2}}\cdot\mathbf{PF}\left(\frac{1}{\cos^2\varphi-\zeta^2}\right)\mathrm{d}\zeta. \tag{81}$$

Equation (80) shows that the radial displacement at the surface $u_r^{(P)}$ has no angular dependence. Also, the other component $u_\varphi^{(P)}$ is anti-symmetric w.r.t. the axes x and y, and vanishes along lines on the surface defined by the angles $\varphi = 0, \pi/2, \pi, 3\pi/2$.

7.2. TANGENTIAL DISPLACEMENTS DUE TO THE TANGENTIAL LOAD S

In the present case, the solution to the second auxiliary problem does play a role. Indeed, solutions (32) and (35) for $\tilde{u}_q^{(S)}$ and $\tilde{u}_s^{(S)}$, respectively, provide through (38) the Radon transformed displacements

$$\tilde{u}_x^{(S)}(q,\omega,z=0) = -\frac{S}{\mu}\big[Q_1(M_{\mathrm{T}}\cos\omega)\sin^2\omega - G^{(S)}(M_{\mathrm{T}}\cos\omega)\cdot\cos^2\omega\big] \times \ln|q|, \tag{82}$$

$$\tilde{u}_y^{(S)}(q,\omega,z=0) = \frac{S\cos\omega\cdot\sin\omega}{\mu}\big[Q_1(M_{\mathrm{T}}\cos\omega) + G^{(S)}(M_{\mathrm{T}}\cos\omega)\big]\ln|q|, \tag{83}$$

where the functions of the Mach number M_T, $G^{(S)}$ (M_T) and $Q_1(M_T)$ are given in (34) and (36), respectively. Then, the latter equations along with (10), (41) and (44) lead to the tangential displacements in the subsonic range

$$u_x^{(S)}(r, \varphi, z = 0) = \frac{S}{2\mu r}\big[Q_{11}(M_T \sin\varphi)\cos^2\varphi - G^{(S)}(M_T \sin\varphi)\sin^2\varphi\big], \tag{84}$$

$$u_y^{(S)}(r, \varphi, z = 0) = \frac{S \cdot \cos\varphi \cdot \sin\varphi}{2\mu r}\big[Q_{11}(M_T \sin\varphi) + G^{(S)}(M_T \sin\varphi)\big]. \tag{85}$$

In addition, applying (39) to (84) and (85) yields

$$u_r^{(S)}(r, \varphi, z = 0) = \frac{S\cos\varphi}{2\mu r} Q_{11}(M_T \sin\varphi), \tag{86}$$

$$u_\varphi^{(S)}(r, \varphi, z = 0) = \frac{S\sin\varphi}{2\mu r} G^{(S)}(M_T \sin\varphi). \tag{87}$$

In what follows, the sub-Rayleigh and the super-Rayleigh/subsonic cases will be treated separately.

7.2.1. *Sub-Rayleigh Range* $(0 < V < V_R)$

Here, the displacements can be calculated from (84)–(87). It is of notice that $u_x^{(S)}$ and $u_y^{(S)}$ are symmetric and anti-symmetric, respectively, w.r.t. both axes x and y.

7.2.2. *Super-Rayleigh Subsonic Range* $(V_R < V < V_T)$

In this case, solutions (84) and (85) exhibit singular behavior along the Rayleigh lines, where $R(M_T \sin\varphi) = 0$. The solutions, as they stand, predict *two* Rayleigh 'sectors'; one ahead of the load S and the other behind. Since only trailing Rayleigh waves are acceptable by the pertinent radiation condition, the 'sector' ahead of the load should be eliminated. Following the same reasoning as in the respective case of $u_z^{(P)}$ (see Subsection 6.1), we write the *corrected* solutions as

$$\begin{aligned} u_x^{(S)}(r, \varphi, z = 0) &= \frac{S}{2\mu}\bigg[\frac{1}{r} Q_{11}(M_T \sin\varphi)\cos^2\varphi - G^{(S)}(M_T \sin\varphi)\cdot\sin^2\varphi \\ &\quad + \frac{\Phi}{r\sin(\varphi - \varphi_R)} - \frac{\Phi}{r\sin(\varphi + \varphi_R)}\bigg], \end{aligned} \tag{88}$$

$$\begin{aligned} u_y^{(S)}(r, \varphi, z = 0) &= \frac{S\cos\varphi\cdot\sin\varphi}{2\mu}\bigg[\frac{1}{r} Q_{11}(M_T \sin\varphi) + G^{(S)}(M_T \sin\varphi) \\ &\quad + \frac{\Psi}{r\sin(\varphi - \varphi_R)} + \frac{\Psi}{r\sin(\varphi + \varphi_R)}\bigg], \end{aligned} \tag{89}$$

where the constants Φ and Ψ are determined by imposing the elimination of the leading Rayleigh-wave 'sectors'. The final expressions read

$$u_x^{(S)}(r,\varphi,z=0) = \frac{S}{2\mu r}\Bigg[Q_{11}(M_{\mathrm{T}}\sin\varphi)\cos^2\varphi - G^{(S)}(M_{\mathrm{T}}\sin\varphi)\sin^2\varphi + \frac{\cos\varphi\cdot m_1(1-m_1)^{1/2}[(2-m_1)^2+4(1-m_1)^{1/2}(1-m^{-2}m_1)^{1/2}]}{\pi M_{\mathrm{T}}(M_{\mathrm{T}}^2\sin^2\varphi-m_1)(M_{\mathrm{T}}^2-m_1)^{1/2}(m_1-m_2)(m_1-m_3)}\Bigg], \tag{90}$$

$$u_y^{(S)}(r,\varphi,z=0) = \frac{S\cos\varphi\cdot\sin\varphi}{2\mu r}\Bigg[Q_{11}(M_{\mathrm{T}}\sin\varphi) + G^{(S)}(M_{\mathrm{T}}\sin\varphi) - \frac{(M_{\mathrm{T}}^2-m_1)^{1/2}(1-m_1)^{1/2}[(2-m_1)^2+4(1-m_1)^{1/2}(1-m^{-2}m_1)^{1/2}]}{\pi\cos\varphi\cdot M_{\mathrm{T}}(M_{\mathrm{T}}^2\sin^2\varphi-m_1)(m_1-m_2)(m_1-m_3)}\Bigg] \tag{91}$$

Finally, the transformation (39) when applied to (86) and (87) provides the displacement components

$$u_r^{(S)}(r,\varphi,z=0) = \frac{S}{2\mu r}\Bigg[Q_{11}(M_{\mathrm{T}}\sin\varphi)\cos\varphi - \frac{(1-m_1)^{1/2}[(2-m_1)^2+4(1-m_1)^{1/2}(1-m^{-2}m_1)^{1/2}]}{\pi M_{\mathrm{T}}(M_{\mathrm{T}}^2-m_1)^{1/2}(m_1-m_2)(m_1-m_3)}\Bigg], \tag{92}$$

$$u_\varphi^{(S)}(r,\varphi,z=0) = \frac{S\sin\varphi}{2\mu r}\Bigg[G^{(S)}(M_{\mathrm{T}}\sin\varphi) - \frac{\cos\varphi M_{\mathrm{T}}(1-m_1)^{1/2}[(2-m_1)^2+4(1-m_1)^{1/2}(1-m^{-2}m_1)^{1/2}]}{\pi(M_{\mathrm{T}}^2-m_1)^{1/2}(m_1-m_2)(m_1-m_3)(M_{\mathrm{T}}^2\sin^2\varphi-m_1)}\Bigg], \tag{93}$$

where one may notice that Rayleigh singular lines do not appear in $u_r^{(S)}$ and that $u_\varphi^{(S)}$ is anti-symmetric w.r.t. the x-axis.

8. The Limit Cases of the Boussinesq and Cerruti Problems

As a check of our method and results, we obtain now the solutions to the problems of Boussinesq and Cerruti as limit cases of our solutions. These classical elastostatic problems involve a 3D half-space under the action of a stationary concentrated load on the surface (see for solutions in, e.g., [35, 26, 36, 37]). The load is either vertical (Boussinesq problem) with magnitude P or tangential (Cerruti problem) with magnitude S.

Here, the above solutions are obtained by allowing $V = 0$, i.e., by considering stationary loads.

Boussinesq's Problem

Equations (47) and (49) provide

$$u_z^{(P)}(r, \varphi, z = 0) = -\frac{P}{2\mu\pi r}\left(1 - M_{\mathrm{L}}^2 \sin^2\varphi\right)^{1/2} \times \frac{[(2 - M_{\mathrm{T}}^2 \sin^2\varphi)^2 + 4(1 - M_{\mathrm{L}}^2 \sin^2\varphi)^{1/2}(1 - M_{\mathrm{T}}^2 \sin^2\varphi)^{1/2}]}{(M_{\mathrm{T}}^2 \sin^2\varphi - m_1)(M_{\mathrm{T}}^2 \sin^2\varphi - m_2)(M_{\mathrm{T}}^2 \sin^2\varphi - m_3)}. \quad (94)$$

Setting $M_{\mathrm{T}} = 0$ and using (A.5) and (27b), we obtain the following expression:

$$u_z^{(P)}(r, \varphi, z = 0) = \frac{P(1 - \nu)}{2\mu\pi r}. \quad (95)$$

Regarding now the radial and tangential displacement components, equations (80) and (81) with $M_{\mathrm{T}} = 0$ give

$$u_r^{(P)}(r, \varphi, z = 0) = -\frac{P}{\mu\pi^2 r}\frac{8m^{-2}}{m_1 m_2 m_3}\int_0^1 \frac{1}{(1 - \zeta^2)^{1/2}}\,\mathrm{d}\zeta, \quad (96)$$

and

$$u_\varphi^{(P)}(r, \varphi, z = 0) = \frac{P \cdot \cos\varphi \cdot \sin\varphi}{\mu\pi^2 r}\frac{8m^{-2}}{m_1 m_2 m_3}\int_0^1 \frac{1}{(1 - \zeta^2)^{1/2}} \times \mathbf{PF}\left(\frac{1}{\cos^2\varphi - \zeta^2}\right)\mathrm{d}\zeta, \quad (97)$$

where $m = [2(1 - \nu)/(1 - 2\nu)]^{1/2}$ (see the definition in (27b)). An analytical evaluation by MATHEMATICA™ shows that the integral in (96) gives the value $\pi/2$, whereas the integral in (97) equals zero for all angles φ with $\cos^2\varphi \neq 1$. In the case $\cos^2\varphi = 1$, despite the hypersingular character of the integrand at the upper limit, $u_\varphi^{(P)}$ becomes zero because of the factor $\sin\varphi$. In view of the above, the final expressions read

$$u_r^{(P)}(r, \varphi, z = 0) = -\frac{P(1 - 2\nu)}{4\mu\pi r}, \quad (98)$$

$$u_\varphi^{(P)}(r, \varphi, z = 0) = 0. \quad (99)$$

Cerruti's Problem

Equations (64), (A.5), (27b) and $M_{\mathrm{T}} = 0$ provide

$$u_z^{(S)}(r, \varphi, z = 0) = \frac{S\cos\varphi}{4\mu\pi r}(1 - 2\nu), \quad (100)$$

whereas (86), (87) and $M_{\mathrm{T}} = 0$ lead to the additional results

$$u_r^{(S)}(r, \varphi, z = 0) = \frac{S \cos \varphi}{2\mu\pi r}, \tag{101}$$

$$u_\varphi^{(S)}(r, \varphi, z = 0) = -\frac{S \sin \varphi}{2\mu\pi r}(1 - \nu). \tag{102}$$

9. Numerical Results and Concluding Remarks

The numerical results are presented in the form of graphs showing the normalized dimensionless displacements

$$\begin{aligned} U_z^{(P)} &= u_z^{(P)} \mu r/P, \quad U_z^{(S)} = u_z^{(S)} \mu r/S, \quad U_z^{(T)} = u_z^{(T)} \mu r/T, \\ U_r^{(P)} &= u_r^{(P)} \mu r/P, \quad U_\varphi^{(P)} = u_\varphi^{(P)} \mu r/P, \quad U_r^{(S)} = u_r^{(S)} \mu r/S \quad \text{and} \\ U_\varphi^{(S)} &= u_\varphi^{(S)} \mu r/S \end{aligned}$$

as functions of the polar angle φ or the shear Mach number M_{T}, for a material with Poisson's ratio $\nu = 0.2$. All integrals appearing in the results of Sections 6 and 7 were evaluated numerically by MATHEMATICA™.

Figure 8 shows $U_z^{(P)}$ vs. φ curves for various load speeds. In the sub-Rayleigh range (case of $M_{\mathrm{T}} = 0.8$) the displacement is positive and, therefore, is directed

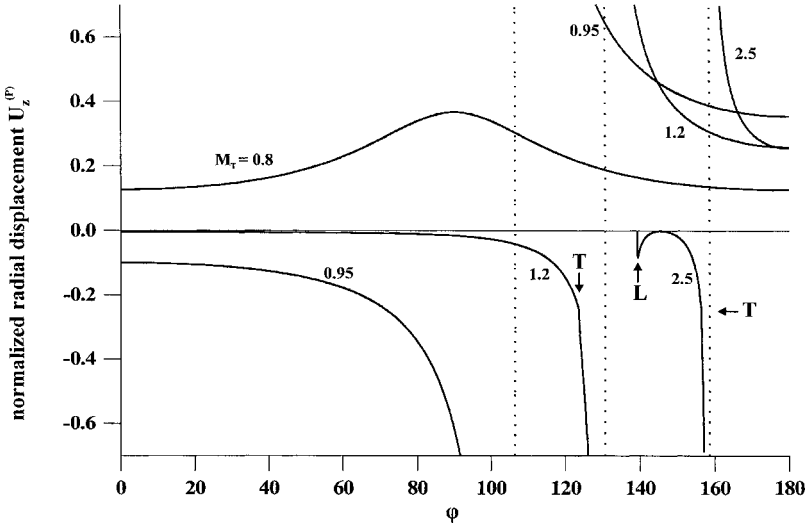

Figure 8. Variation of the normalized vertical displacement $U_z^{(P)} = u_z^{(P)} \mu r/P$, due to a normal moving load, with the polar angle φ for various load speeds (cases of $M_{\mathrm{T}} = 0.8$, $M_{\mathrm{T}} = 0.95$, $M_{\mathrm{T}} = 1.2$ and $M_{\mathrm{T}} = 2.5$ – which correspond to sub-Rayleigh, super-Rayleigh/subsonic, transonic and supersonic motion, respectively). The symbols L and T mark discontinuities associated with longitudinal and transverse (shear) wavefronts, respectively.

into the half-space. In the subsonic/super-Rayleigh range (case of $M_T = 0.95$), there is a Cauchy-type discontinuity along the Rayleigh Mach wavefronts at $\varphi = 106.47°$ and the displacement is positive in the sector defined by the Rayleigh lines (behind the load) but negative elsewhere. In the transonic range (case of $M_T = 1.2$), there is a Cauchy-type discontinuity along the Rayleigh wavefronts at $\varphi = 130.61°$ and a slope discontinuity along the shear wavefronts (defined by $M_T^2 \sin^2 \varphi = 1$) at $\varphi = 123.56°$. In the supersonic range (case of $M_T = 2.5$), the displacement suffers a Cauchy-type discontinuity along the Rayleigh wavefronts at $\varphi = 158.63°$ and a slope discontinuity along the shear wavefronts at $\varphi = 156.42°$. In the same range, the displacement becomes zero along the longitudinal wavefronts at $\varphi = 139.22°$.

Figures 9, 10, 11 and 12 show $U_z^{(S)}$ vs. φ curves for, respectively, a sub-Rayleigh speed of the load S ($M_T = 0.8$), a super-Rayleigh/subsonic speed ($M_T = 0.95$), a transonic speed ($M_T = 1.2$) and a supersonic speed ($M_T = 2.5$). It is of notice in the super-Rayleigh/subsonic case that $U_z^{(S)}$ is continuous along the Rayleigh lines at $\varphi = 106.47°$ and that the magnitude of $U_z^{(S)}$ is smaller (by a factor of 10, approximately) in the super-Rayleigh case as compared to that in the sub-Rayleigh case. Also $U_z^{(S)}$ is symmetric w.r.t. the x-axis and is zero along lines at $\varphi = \pi/2, 3\pi/2$. In the transonic case, $U_z^{(S)}$ experiences a slope discontinuity at the shear Mach wavefronts and, also, it is negative inside the shear wavefront sector but positive outside this sector. Finally, Figure 12 shows that $U_z^{(S)}$ in the supersonic case is zero everywhere except in the two sectors between the longitudinal and shear wavefront lines.

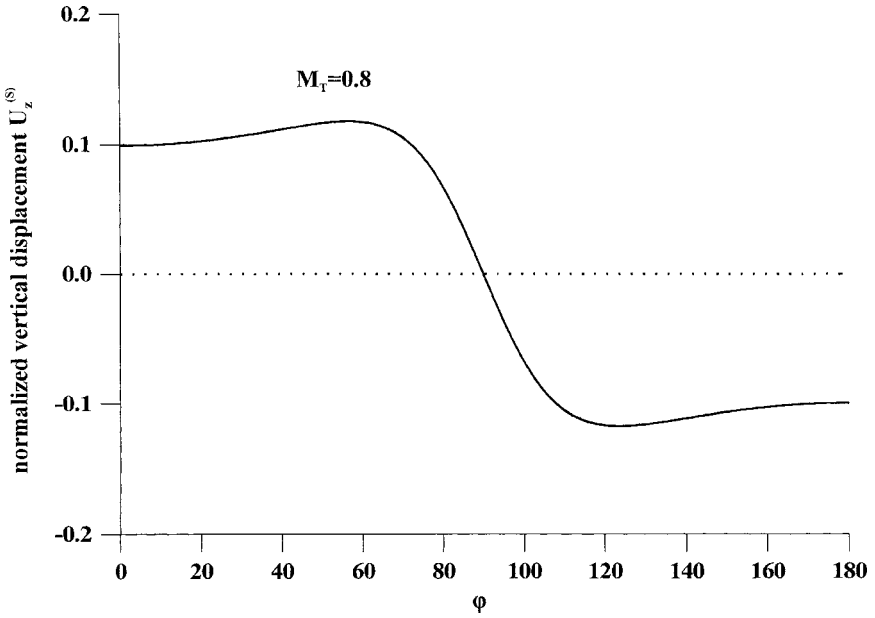

Figure 9. Variation of the normalized vertical displacement $U_z^{(S)} = u_z^{(S)} \mu r/S$, due to a tangential moving load, with the polar angle φ for a load speed $M_T = 0.8$.

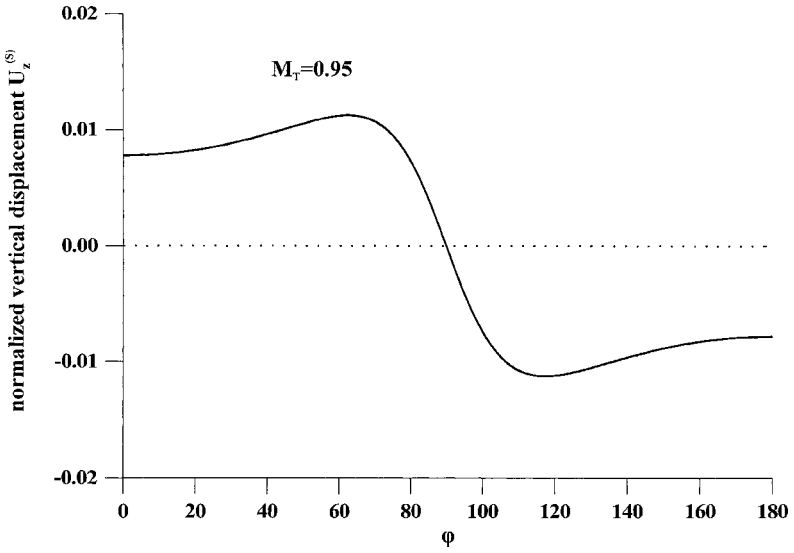

Figure 10. Variation of the normalized vertical displacement $U_z^{(S)} = u_z^{(S)}\mu r/S$, due to a tangential moving load, with the polar angle φ for a load speed $M_T = 0.95$.

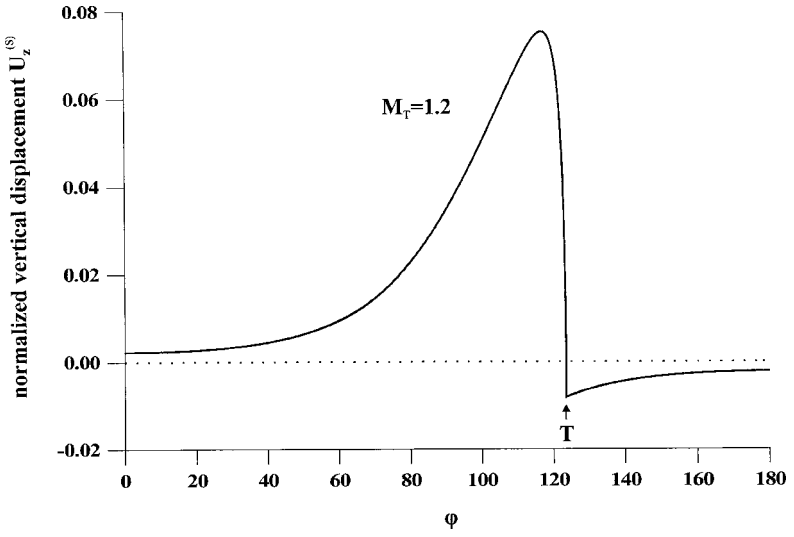

Figure 11. Variation of the normalized vertical displacement $U_z^{(S)} = u_z^{(S)}\mu r/S$, due to a tangential moving load, with the polar angle φ for a load speed $M_T = 1.2$.

Figure 13 depicts the variation of $U_z^{(T)}$ with φ for the speed values $M_T = 0.8$ (sub-Rayleigh range) and $M_T = 0.95$ (super-Rayleigh/subsonic range) of the load T. It is worth noticing that the vertical displacement becomes zero at $\varphi = \pi/2$ and $\varphi = 3\pi/2$. This can be explained physically since, at these angles, the 3D

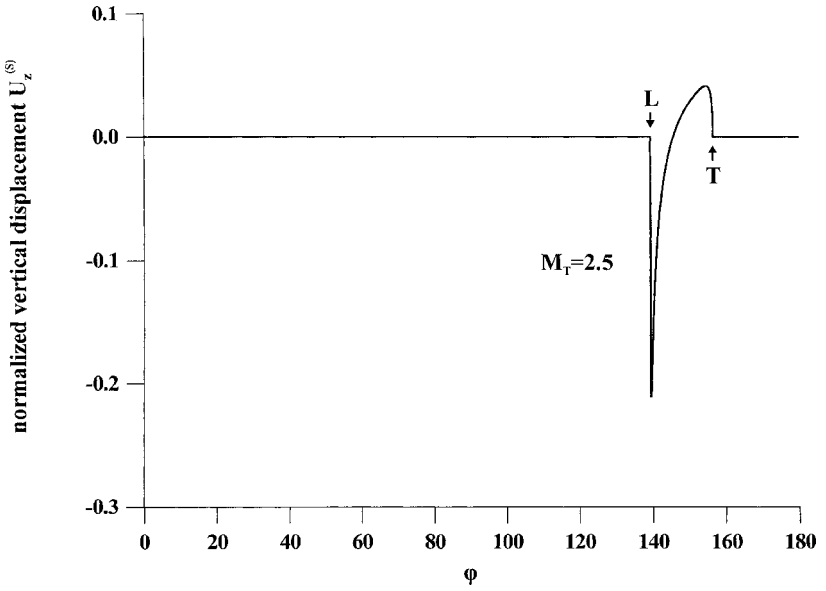

Figure 12. Variation of the normalized vertical displacement $U_z^{(S)} = u_z^{(S)}\mu r/S$, due to a tangential moving load, with the polar angle φ for a load speed $M_T = 2.5$.

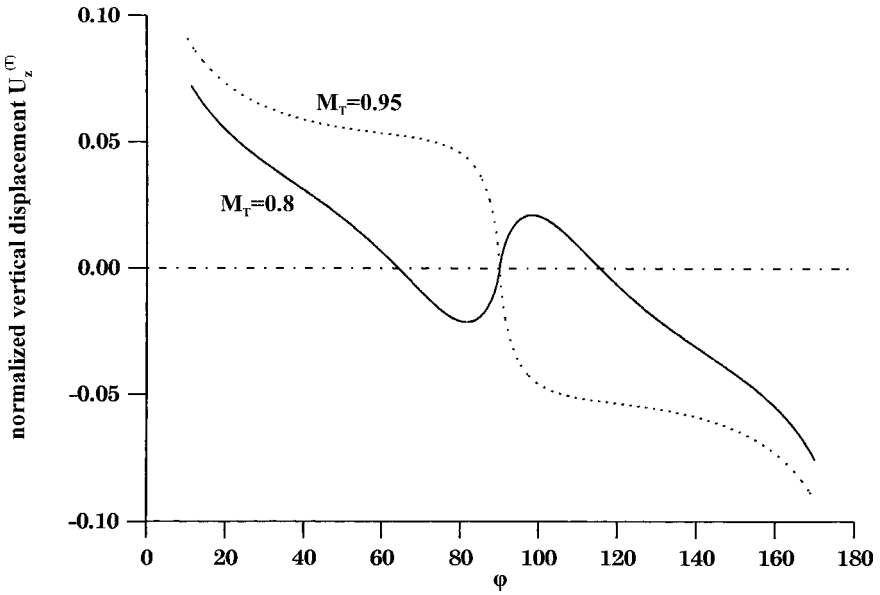

Figure 13. Variation of the normalized vertical displacement $U_z^{(T)} = u_z^{(T)}\mu r/T$, due to a tangential moving load having a direction orthogonal to the direction of motion, with the polar angle φ for load speeds $M_T = 0.8$ and $M_T = 0.95$.

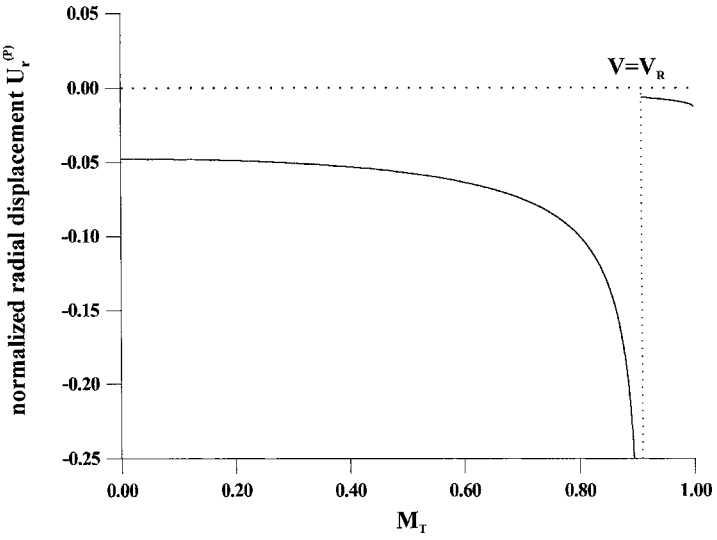

Figure 14. Variation of the normalized radial displacement $U_r^{(P)} = u_r^{(P)}\mu r/P$, due to a normal moving load, with the transverse Mach number M_{T}. The discontinuity occurs when the load speed reaches the Rayleigh wave speed in the medium ($V = V_{\mathrm{R}}$).

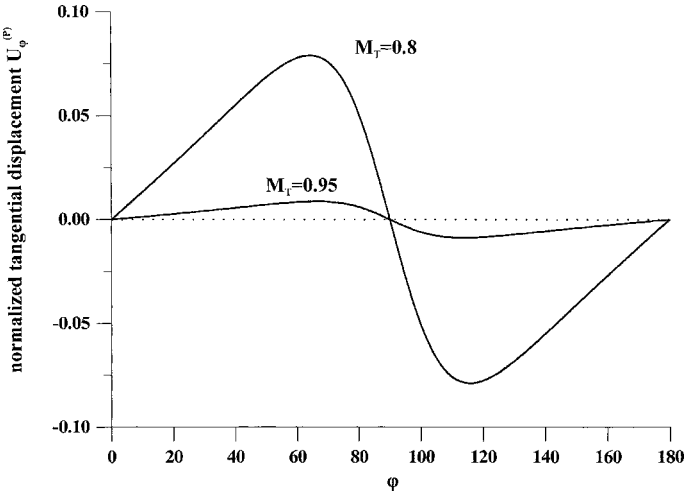

Figure 15. Variation of the normalized tangential displacement $U_\varphi^{(P)} = u_\varphi^{(P)}\mu r/P$, due to a normal moving load, with the polar angle φ for load speeds $M_{\mathrm{T}} = 0.8$ and $M_{\mathrm{T}} = 0.95$.

problem with the T force acting normal to the xz-plane degenerates into a 2D problem of anti-plane shear deformation in the xz-plane.

Figure 14 shows the variation of $U_r^{(P)}$ with the Mach number M_{T} in the subsonic range, where $U_r^{(P)}$ is independent of the polar angle φ. The radial displacement is negative (i.e., its direction is towards the point of application of the load) and becomes infinite as the velocity approaches the Rayleigh wave velocity at $V_{\mathrm{R}}/V_{\mathrm{T}} \cong$

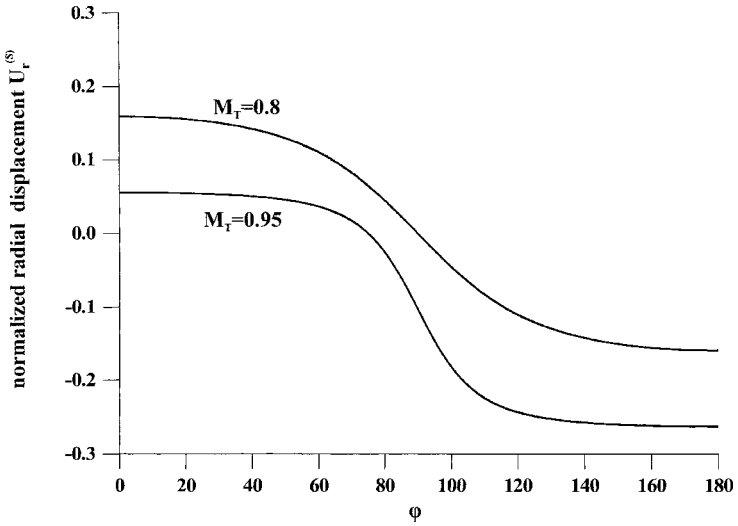

Figure 16. Variation of the normalized radial displacement $U_r^{(S)} = u_r^{(S)}\mu r/S$, due to a tangential moving load, with the polar angle φ for load speeds $M_T = 0.8$ and $M_T = 0.95$.

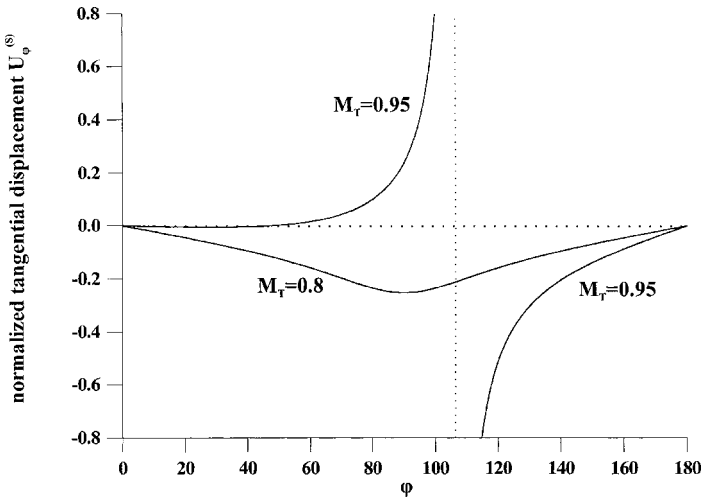

Figure 17. Variation of the normalized tangential displacement $U_\varphi^{(S)} = u_\varphi^{(S)}\mu r/S$, due to a tangential moving load, with the polar angle φ for $M_T = 0.8$ and $M_T = 0.95$.

0.91. At this speed the displacement is discontinuous. When $V_R < V$, $U_r^{(P)}$ is finite everywhere and remains continuous across the Rayleigh lines. Figure 15 shows the variation of $U_\varphi^{(P)}$ with φ indicating that this displacement component is continuous across the Rayleigh lines, the x-axis and the y-axis. $U_\varphi^{(P)}$ is anti-symmetric w.r.t. the x and y axes. Also, one may observe that the magnitude of $U_\varphi^{(P)}$ is much smaller in the super-Rayleigh speed (case of $M_T = 0.95$) than the one in the sub-Rayleigh speed (case of $M_T = 0.8$).

Figure 16 shows the variation of $U_r^{(S)}$ with φ at load velocities $M_T = 0.8$ and $M_T = 0.95$. No Rayleigh singularity appears and $U_r^{(S)}$ is continuous and bounded in all directions. Figure 17 depicts $U_\varphi^{(S)}$ vs. φ indicating that this displacement component: (i) is continuous in the entire φ range, (ii) is negative in the half-plane $y > 0$ and positive in the half-plane $y < 0$, in the case of sub-Rayleigh speeds ($M_T = 0.8$), and (iii) suffers a Cauchy-type singularity at the Rayleigh wavefront, in the case of super-Rayleigh speeds ($M_T = 0.95$).

In closing, we notice that the present results can also be used as Green's functions to accomplish *integral-equation* solutions for 3D elastodynamic contact problems, in the manner employed in, e.g., [1, 38] for simpler 2D problems. Indeed, relative efforts by the authors are underway.

Appendix A

Following concepts from Rahman and Barber [30], we write the function $K(M_T)$, which is defined in (29b), as

$$\begin{aligned} K(M_T) &= M_T^2\big[M_T^6 - 8M_T^4 + 8\big(3 - 2m^{-2}\big)M_T^2 - 16\big(1 - m^{-2}\big)\big] \\ &= M_T^2\big(M_T^2 - m_1\big)\big(M_T^2 - m_2\big)\big(M_T^2 - m_3\big), \end{aligned} \tag{A.1}$$

where (m_1, m_2, m_3) are the nontrivial zeros of $K(M_T)$. Now, we depart from the analysis of Rahman and Barber [30] and fully exploit the potentiality of MATHEMATICA™ as a symbolic algebra program obtaining the following expressions for these zeros

$$m_1 = \frac{4}{3}\left[2 + \frac{2^{1/3}(5\nu - 2)}{\beta(\nu)} - \frac{2^{2/3}}{4(1-\nu)}\beta(\nu)\right], \tag{A.2}$$

$$m_2 = \frac{2}{3}\left[4 - \frac{2^{1/3}(1 + \mathrm{i}3^{1/2})(5\nu - 2)}{\beta(\nu)} + \frac{2^{2/3}(1 - \mathrm{i}3^{1/2})}{4(1-\nu)}\beta(\nu)\right], \tag{A.3}$$

$$m_3 = \frac{2}{3}\left[4 - \frac{2^{1/3}(1 - \mathrm{i}3^{1/2})(5\nu - 2)}{\beta(\nu)} + \frac{2^{2/3}(1 + \mathrm{i}3^{1/2})}{4(1-\nu)}\beta(\nu)\right], \tag{A.4}$$

where ν is Poisson's ratio, $\mathrm{i} = (-1)^{1/2}$,

$$\beta(\nu) = \big[3^{3/2}\gamma(\nu) + 56\nu^3 - 123\nu^2 + 78\nu - 11\big]^{1/3},$$

and

$$\gamma(\nu) = \big[(1-\nu)^3(32\nu^3 - 16\nu^2 + 21\nu - 5)\big]^{1/2}.$$

Further, an inspection on the above functions with MATHEMATICA™ and a graphical representation of the functions $m_1(\nu)$, $\mathrm{Re}\{m_2(\nu)\}$ and $\mathrm{Re}\{m_3(\nu)\}$, where $\mathrm{Re}\{\cdot\}$ denotes the real part of a complex function, reveal the following:

(i) The zero m_1 is real for all values of ν and coincides with the nontrivial zero of the Rayleigh function $R(M_T)$.

(ii) The zeros m_2 and m_3 are also zeros of the function $(2 - M_T^2)^2 + 4(1 - M_L^2)^{1/2} \times (1 - M_T^2)^{1/2}$. They are real in the interval $0 < \nu \leqslant \nu_0$, where $\nu_0 = 0.2630820648\ldots$, and complex conjugate in the interval $\nu_0 < \nu < 0.5$. We also notice that ν_0 is the real zero of $\gamma(\nu)$.

(iii) The inequalities $m_1 < 1 < \mathrm{Re}\{m_2\} < \mathrm{Re}\{m_3\}$ are valid.

(iv) The inequalities $M_L^2 < M_T^2 \leqslant m^2 < m_2 < m_3$ are valid in the subsonic and transonic speed ranges, if, of course, (m_2, m_3) are real (i.e., for Poisson's ratios in the interval $0 < \nu \leqslant \nu_0$).

(v) The equality $m_1 m_2 m_3 = 16(1 - m^{-2})$ is always valid.

By having available, through (A.1), the factorization forms of $K(V_T)$ and $R(V_T)$ permits writing (49) and other analogous equations in the main text of the paper.

This appendix presents also the expansions of the functions (A, B, C, D) in sums of partial fractions. These are as follows

$$A(M_T) \equiv \frac{4(1 - M_L^2)}{\prod_{j=1}^{3}(M_T^2 - m_j)} = \sum_{j=1}^{3} \frac{A_j}{(M_T^2 - m_j)}, \tag{A.5}$$

$$B(M_T) \equiv \frac{(2 - M_T^2)^2}{\prod_{j=1}^{3}(M_T^2 - m_j)} = \sum_{j=1}^{3} \frac{B_j}{(M_T^2 - m_j)}, \tag{A.6}$$

$$C(M_T) \equiv \frac{(8m^{-2} - 4) + (6 - 8m^{-2})M_T^2 - M_T^4}{\prod_{j=1}^{3}(M_T^2 - m_j)} = \sum_{j=1}^{3} \frac{C_j}{(M_T^2 - m_j)}, \tag{A.7}$$

$$D(M_T) \equiv \frac{2(2 - M_T^2)}{\prod_{j=1}^{3}(M_T^2 - m_j)} = \sum_{j=1}^{3} \frac{D_j}{(M_T^2 - m_j)}, \tag{A.8}$$

where

$$A_1 = \frac{4(1 - m^{-2}m_1)}{(m_1 - m_2)(m_1 - m_3)}, \quad A_2 = \frac{4(1 - m^{-2}m_2)}{(m_2 - m_1)(m_2 - m_3)}, \quad A_3 = \frac{4(1 - m^{-2}m_3)}{(m_3 - m_1)(m_3 - m_2)}, \tag{A.9a,b,c}$$

$$B_1 = \frac{(2 - m_1)^2}{(m_1 - m_2)(m_1 - m_3)}, \quad B_2 = \frac{(2 - m_2)^2}{(m_2 - m_1)(m_2 - m_3)}, \quad B_3 = \frac{(2 - m_3)^2}{(m_3 - m_1)(m_3 - m_2)}, \tag{A.10a,b,c}$$

$$C_1 = \frac{(8m^{-2} - 4) + (6 - 8m^{-2})m_1 - m_1^2}{(m_1 - m_2)(m_1 - m_3)},$$

$$C_2 = \frac{(8m^{-2} - 4) + (6 - 8m^{-2})m_2 - m_2^2}{(m_2 - m_1)(m_2 - m_3)}, \tag{A.11a,b,c}$$

$$C_3 = \frac{(8m^{-2} - 4) + (6 - 8m^{-2})m_3 - m_3^2}{(m_3 - m_1)(m_3 - m_2)},$$

$$D_1 = \frac{2(2-m_1)}{(m_1-m_2)(m_1-m_3)}, \quad D_2 = \frac{2(2-m_2)}{(m_2-m_1)(m_2-m_3)}, \quad D_3 = \frac{2(2-m_3)}{(m_3-m_1)(m_3-m_2)}. \tag{A.12a,b,c}$$

Appendix B

The solution to the second auxiliary problem described by (14), (16) and (19), i.e., the 2D anti-plane shear problem of a moving load, is effected through the use of the two-sided Laplace transform and exact inversions involving contour integration. The two-sided Laplace transform pair is written as

$$U_s(p,\omega,z) = \int_{-\infty}^{+\infty} \tilde{u}_s(q,\omega,z)\cdot \mathrm{e}^{-pq}\,\mathrm{d}q, \quad \tilde{u}_s(q,\omega,z) = \frac{1}{2\pi \mathrm{i}}\int_{Br} U_s(p,\omega,z)\cdot \mathrm{e}^{pq}\,\mathrm{d}p, \tag{B.1a,b}$$

where Br denotes the Bromwich inversion path in the complex p-plane. Operating now with (B.1a) on (14) gives

$$\frac{\mathrm{d}^2 U_s}{\mathrm{d}z^2} + \left(1-m^2c_x^2\right)p^2 U_s = 0, \tag{B.2}$$

where one may discern the following two cases: (i) $1-m^2c_x^2 > 0 \Leftrightarrow |V\cdot\cos\omega| < V_{\mathrm{T}}$, and (ii) $1-m^2c_x^2 < 0 \Leftrightarrow |V\cdot\cos\omega| > V_{\mathrm{T}}$. The first and second inequalities define, respectively, the subsonic and supersonic velocity ranges.

The subsonic case is considered first. To facilitate the definition of the pertinent branch cuts in the complex p-plane (these branch cuts are needed in order for us to have a *bounded* solution as $z\to\infty$), we write (B.2) as $(\mathrm{d}^2U_s/\mathrm{d}z^2) - (1-m^2c_x^2)(\varepsilon^2-p^2)U_s = 0$, where ε is a real positive number such that $\varepsilon\to 0$ (see for this standard procedure in, e.g., [39, 40]). In this way, the latter ODE supplied with the transformed boundary condition (16) has the following (bounded) solution $U_s(p,\omega,z) = -(S\cdot\sin\omega/\mu b)\cdot\exp(-bz)$, where $b \equiv b(p) = (1-m^2c_x^2)^{1/2}(\varepsilon^2-p^2)^{1/2}$ and $\mathrm{Re}(b) > 0$ in the p-plane with cuts along the intervals $\varepsilon < |\mathrm{Re}(p)| < \infty, \mathrm{Im}(p) = 0$. The transformed solution shows that U_s is an analytic function of p when $\mathrm{Re}(p) = 0$ and, therefore, the inversion can be effected through the operation

$$\tilde{u}_s(q,\omega,z) = -\frac{S\sin\omega}{\mathrm{i}2\pi\mu}\int_{-\mathrm{i}\infty}^{+\mathrm{i}\infty}\frac{\mathrm{e}^{-bz}}{b}\,\mathrm{e}^{pq}\,\mathrm{d}p. \tag{B.3}$$

By deforming now the original integration path onto a contour that includes large quarter-circular paths at infinity in the $\mathrm{Re}(p) < 0$ half-plane and straight paths along the pertinent branch cut, and exploiting Cauchy's theorem along with

Jordan's lemma, we obtain the following result in terms of a *real* integral in the case $q \geqslant 0$ (in the other case $q \leqslant 0$, an analogous expression is obtained by deforming the integration path in the $\mathrm{Re}(p) > 0$ half-plane)

$$\tilde{u}_s(q, \omega, z = 0) = -\frac{S \sin \omega}{\pi \mu (1 - m^2 c_x^2)^{1/2}} \int_{\varepsilon}^{\infty} \frac{\mathrm{e}^{-pq}}{(p^2 - \varepsilon^2)^{1/2}} \, \mathrm{d}p,$$
$$\text{with } q \geqslant 0. \tag{B.4}$$

From entry 3.387.6 in the Table of Gradshteyn and Ryzhik [41] or by using MATHEMATICA™, the integral is found to be $K_0(\varepsilon q)$, where K_0 is the modified Bessel function of order zero. K_0 behaves as $\lim_{x \to 0} K_0(x) = -\ln |x|$ (see, e.g., [42]). In the present case, of course, $\varepsilon \to 0$ so that one may write

$$K_0(\varepsilon q) = -\ln \big(\varepsilon |q|\big) = -\ln(\varepsilon) - \ln \big(|q|\big), \quad \text{with } \varepsilon \to 0. \tag{B.5}$$

But, at this point, it proves useful to recall that $\tilde{u}_s(q, \omega, z = 0)$ in (B.4) expresses *displacement*. In (B.5), therefore, the spatially independent term $\ln(\varepsilon)$ can be identified with a *rigid-body* displacement and, consequently, be omitted from the final expression providing the displacement. An extensive discussion of the latter argument can be found in [40], and here we just mention that the occurrence of $\ln(\varepsilon)$ in (B.5) simply confirms the well-known result that the solution of the Neumann boundary value problem for an elliptic PDE (as is (14) in the subsonic regime) is unique up to an *arbitrary* constant.

In view of the above, the solution of the second auxiliary problem in the subsonic range (i.e., $|V \cos \omega| < V_{\mathrm{T}}$) is given as

$$\tilde{u}_s(q, \omega, z = 0) = \frac{S \cdot \sin \omega}{\pi \mu (1 - m^2 c_x^2)^{1/2}} \ln |q|. \tag{B.6}$$

For the supersonic case next, we find that the general solution of the ODE in (B.2) has the form

$$U_s(p, \omega, z) = L_1 \exp\big[-(m^2 c_x^2 - 1)^{1/2} pz\big] + L_2 \exp\big[(m^2 c_x^2 - 1)^{1/2} pz\big],$$

where (L_1, L_2) are constants to be determined through enforcement of the boundary conditions. Since by the radiation condition (see e.g., [26]) only *backward* running waves (i.e., waves trailing from the moving source) are admitted, the first term in the aforementioned general solution is rejected because it would result in disturbances moving ahead of the source. Indeed, one may observe that multiplying the term $L_2 \exp[(m^2 c_x^2 - 1)^{1/2} pz]$ by the term $\exp(pq)$ appearing in the inverse Laplace transform in (B.1b) gives the solution form $L_2 \exp[\mathrm{iIm}(p) \cdot (q + (m^2 c_x^2 - 1)^{1/2} z)]$, which is consistent with the physical condition that for $|V \cdot \cos \omega| > V_{\mathrm{T}}$ the medium in front of the source is not disturbed, the term containing $(q - (m^2 c_x^2 - 1)^{1/2} z)$ being rejected from the solution.

In view of the above and the transformed boundary condition, the solution $U_s(p, \omega, z = 0)$ is found to be

$$U_s(p, \omega, z = 0) = \frac{S \sin \omega}{\mu (m^2 c_x^2 - 1)^{1/2}} \frac{1}{p}, \tag{B.7}$$

whereas its inverse $\tilde{u}_s(q, \omega, z = 0)$ is evaluated through standard Tables and has the form

$$\tilde{u}_s(q, \omega, z = 0) = \frac{S \sin \omega}{2\mu(m^2 c_x^2 - 1)^{1/2}} \cdot \mathrm{sgn}(q). \tag{B.8}$$

Finally, since the relation $\mathrm{sgn}(q) = 1 - 2H(-q)$ holds between the signum and Heaviside functions, the solution of the second auxiliary problem in the supersonic range (i.e., $|V \cdot \cos \omega| > V_{\mathrm{T}}$) is given as

$$\tilde{u}_s(q, \omega, z = 0) = -\frac{S \sin \omega}{\mu(m^2 c_x^2 - 1)^{1/2}} \cdot H(-q), \tag{B.9}$$

where, again, the rigid-body term is omitted.

References

1. H.G. Georgiadis and J.R. Barber, On the super-Rayleigh/subseismic elastodynamic indentation problem. *J. Elasticity* **31** (1993) 141–161.
2. J.R. Barber and M. Ciavarella, Contact mechanics. *Internat. J. Solids and Structures* **37** (2000) 29–43.
3. Y. Huang, W. Wang, C. Liu and A.J. Rosakis, Intersonic crack growth in bimaterial interfaces: An investigation of crack face contact. *J. Mech. Phys. Solids* **46** (1998) 2233–2259.
4. G. Lefeuvemesgouez, D. Lehouedec and A.T. Peplow, Ground vibration in the vicinity of a high-speed moving harmonic strip load. *J. Sound Vibration* **231** (2000) 1289–1309.
5. V.V. Krylov, A.R. Dawson, M.E. Heelis and A.C. Collop, Rail movement and ground waves caused by high-speed trains approaching track-soil critical velocities. *Proc. of Institution of Mechanical Engineers* (Part F) **214** (2000) 107–116.
6. D.L. Lansing, The displacement in an elastic half-space due to a moving concentrated normal load. NASA Technical Report R-238 (1966).
7. W. Miles, On the response of an elastic half space to a moving blast wave. *ASME J. Appl. Mech.* **27** (1960) 710–716.
8. I.N. Sneddon, Stress produced by a pulse of pressure moving along the surface of a semi-infinite solid. *Rendiconti Circolo Matematico di Palermo* **2** (1952) 57–62.
9. J. Cole and J. Huth, Stresses produced in a half plane by moving loads. *ASME J. Appl. Mech.* **25** (1958) 433–436.
10. H.G. Georgiadis and J.R. Barber, Steady-state transonic motion of a line load over an elastic half-space: The corrected Cole-Huth solution. *ASME J. Appl. Mech.* **60** (1993) 772–774.
11. G. Eason, The stresses produced in semi-infinite solid by a moving surface force. *Internat. J. Engrg. Sci.* **2** (1965) 581–609.
12. J.R. Barber, Surface displacements due to a steadily moving point force. *ASME J. Appl. Mech.* **63** (1996) 245–251.
13. L.M. Brock and M.J. Rodgers, Steady-state response of a thermoelastic half-space to the rapid motion of surface thermal/mechanical loads. *J. Elasticity* **47** (1997) 225–240.
14. I.M. Gelfand, M.I. Graev and N.Ya. Vilenkin, *Generalized Functions*, Vol. 5. Academic Press, New York (1966).
15. D. Ludwig, The Radon transform on Euclidean space. *Commun. Pure Appl. Math.* **19** (1966) 49–81.
16. S.R. Deans, *The Radon Transform and Some of Its Applications.* Wiley, New York (1983).
17. B.W. Roos, *Analytic Functions and Distributions in Physics and Engineering*. Wiley, New York (1969).

18. H.A. Lauwerier, The Hilbert problem for generalized functions. *Arch. Rational Mech. Anal.* **13** (1963) 157–166.
19. R.P. Kanwal, *Generalized Functions: Theory and Technique*. Birkhäuser, Boston (1998).
20. G. Lykotrafitis and H.G. Georgiadis, The three-dimensional steady-state thermo-elastodynamic problem of moving sources over a half-space, in preparation (2001).
21. V.A. Sveklo, Boussinesq type problems for the anisotropic half-space. *J. Appl. Math. Mech.* **28** (1964) 1099–1105.
22. V.B. Poruchikov, *Methods of the Classical Theory of Elastodynamics*. Springer, Berlin (1993).
23. J.R. Willis, The distribution of stress in an anisotropic elastic body containing an exterior crack. *Internat. J. Engrg. Sci.* **8** (1970) 559–574.
24. C.-Y. Wang and J.D. Achenbach, Lamb's problem for solids of general anisotropy. *Wave Motion* **24** (1996) 227–242.
25. S.V. Shmegera, The initial boundary-value mixed problems for elastic half-plane with the conditions of contact friction. *Internat. J. Solids Struct.* **37** (2000) 6277–6296.
26. Y.C. Fung, *Foundations of Solid Mechanics*. Prentice-Hall, Englewood Cliffs, NJ (1965).
27. H.G. Georgiadis, On the stress singularity in steady-state transonic shear crack propagation. *Internat. J. Fracture* **30** (1986) 175–180.
28. M.J. Ablowitz and A.S. Fokas, *Complex Variables: Introduction and Applications*. Cambridge Univ. Press, Cambridge (1997).
29. L.M. Brock and H.G. Georgiadis, Steady-state motion of a line mechanical/heat source over a half-space: a thermoelastodynamic solution. *ASME J. Appl. Mech.* **64** (1997) 562–567.
30. M. Rahman and J.R. Barber, Exact expressions for the roots of the secular equation for Rayleigh waves. *ASME J. Appl. Mech.* **62** (1995) 250–252.
31. R.G. Payton, An application of the dynamic Betti–Rayleigh reciprocal theorem to moving-point loads in elastic media. *Quart. Appl. Math.* **21** (1964) 299–313.
32. D.C. Gakenheimer and J. Miklowitz, Transient excitation of an elastic half space by a point load traveling on the surface. *ASME J. Appl. Mech.* **36** (1969) 505–515.
33. M.C.M. Bakker, B.J. Verweij, B.J. Kooij and H.A. Dieterman, The traveling point load revisited. *Wave Motion* **29** (1999) 119–135.
34. J.R. Willis, Hertzian contact of anisotropic bodies. *J. Mech. Phys. Solids* **14** (1966) 163–176.
35. S.P. Timoshenko and J.N. Goodier, *Theory of Elasticity*. McGraw–Hill, New York (1970).
36. L. Landau and I.M. Lifshitz, *Theory of Elasticity*. Pergamon Press, Oxford (1970).
37. J.R. Barber, *Elasticity*. Kluwer Academic, Dordrecht (1992).
38. L.M. Brock and H.G. Georgiadis, Sliding contact with friction of a thermoelastic solid at subsonic, transonic and supersonic speeds. *J. Thermal Stresses* **23** (2000) 629–656.
39. G.A. Carrier, M. Krook and C.E. Pearson, *Functions of a Complex Variable*. McGraw–Hill, New York (1966).
40. H.G. Georgiadis and I. Vardoulakis, Anti-plane shear Lamb's problem treated by gradient elasticity with surface energy. *Wave Motion* **28** (1998) 353–366.
41. I.S. Gradshteyn and I.M. Ryzhik, *Table of Integrals, Series and Products*. Academic Press, New York (1980).
42. M. Abramowitz and I.A. Stegun, *Handbook of Mathematical Functions*. Dover, New York (1982).